Construction and Building Materials 428 (2024) 136295

Contents lists available at ScienceDirect

Construction and Building Materials

journal homepage: www.elsevier.com/locate/conbuildmat

Development of low carbon concrete and prospective of geopolymer concrete using lightweight coarse aggregate and cement replacement materials

Promise D. Nukah [a,*], Samuel J. Abbey [a,b], Colin A. Booth [a,b], Jonathan Oti [c]

[a] School of Engineering, College of Arts, Technology and Environment, University of the West of England, Bristol BS16 1QY, UK
[b] Centre for Architecture and Built Environment Research (CABER), College of Arts, Technology and Environment, University of the West of England, Bristol BS16 1QY, UK
[c] Faculty of Computing, Engineering and Science, University of South Wales, Pontypridd CF37 1DL, UK

ARTICLE INFO

Keywords:
Green concrete
Embodied carbon
Flexural strength
Lightweight concrete
Geopolymer-concrete creep
Compressive strength

ABSTRACT

The use of Ground Granulated Blast-furnace Slag (GGBS) as an alternative cement replacement material in combination with conventional coarse aggregate have been successful in the production of near green concrete. Undoubtedly, GGBS has exhibited good cementitious attributes, however, there are concerns with slow strength development and workability owing to its non-pozzolanic activities as well as some degree of porosity notwithstanding the sustainability potential. Therefore, this study presents a lytag based geopolymer lightweight concrete with high strength development, improved mechanical properties and reduced embodied carbon. To further improve and enhance the potential production of green concrete, complete replacement of conventional coarse aggregate with a recycled lightweight aggregate from industrial waste was carried out. The geopolymer precursors consisted of sodium hydroxide, sodium silicate, GGBS and silica fume to optimize the performance of the concrete at 60–80% cement replacement for a target design mix of 20, 30, 40, and 50 MPa. The performance of lytag based geopolymer concrete was compared with that of non-geopolymer lytag based concrete (control samples). The results show a 42% increase in compressive strength for the geopolymer lightweight concrete and a 22% increase in ultimate compressive strain which is an indication of improved moment of resistance in structural design. The results also show a 46–61% reduction in embodied carbon for the use of non-geopolymer lytag based concrete and 69–77% reduction for lytag based geopolymer concrete. The geopolymer concrete between 7 and 63 days of loading increases by 0.55% in creep strain compared with increases of 2.81% for non-geopolymer lytag based concrete and reduction to 27.96% for the normal weight concrete. Modulus of Elasticity reduces with age of loading for the geopolymer concrete during creep at 0.39% compared to reduction of 1.93% for non-geopolymer lytag based concrete and increase of 12% for the normal weight concrete.

1. Introduction

Global carbon emission has caught the attention of policy makers due to increase energy demands incident on population growth and the need to reduce the effect on the environment. The construction industry being responsible to provide for infrastructural deficit account for about 6% of global carbon anthropogenic emission for which cement impacts significantly with 900 kg of carbon emission for every 1000 kg of cement produced [1–3]. This necessitates the search for a potential cement replacement in concrete with the aims of lowering the concrete carbon footprint with good structural performance. The impact of low carbon concrete on the environment using materials from industrial waste brings about overwhelming improvement in sustainability hence it is described as green concrete. Green concrete consists of materials whose alternative binders are made of Supplementary Cementitious Material (SCM) having a low impact on carbon emission. The determinant of SCM is based on the ability of the materials to possess certain cementitious and pozzolanic tendencies. The mineralogy of cement reveals that it has high percentage composition of calcium oxide (CaO) which is responsible for its mechanical performance. During the initial stage of concrete development, calcium hydroxide [Ca $(OH)_2$], is formed which is known to initiate concrete strength. Owing to the negative impact of carbon emission associated with cement, an alternative chemical composition is

* Corresponding author.
E-mail address: promise.nukah@uwe.ac.uk (P.D. Nukah).

https://doi.org/10.1016/j.conbuildmat.2024.136295
Received 5 January 2024; Received in revised form 13 April 2024; Accepted 15 April 2024

Nomenclature

CaO	Calcium oxide
GGBS	Ground granular blast furnace slag.
$Ca(OH)_2$	Calcium hydroxide
C-S-H	Calcium silicate hydrate
Al_2SiO_3	Aluminium oxide
SiO_2	Silicon dioxide
A/B	Alkaline binder ratio
PFA	Pulverise Fuel Ash
SEM	Scanning electron microscopy
w/c	Water to binder ratio
SCM	Supplementary cementitious Material
H_2O	Water
OPC	Ordinary Portland Cement
LC	Lightweight Concrete.
SF	Silica Fume
SP	Superplasticizer
GCB	Green Concrete Binder
AS	Alkaline solution
GC	Green Concrete
ASG	Alkaline Silica Gel
ASR	Alkaline Silica Reaction
n	Concrete sample size

sort in a potential alternative binder having aluminium silicate. This has shown to enhance the mechanical properties of green concrete. The use of SCM having aluminium silicate results to compressive strength development through the densification of concrete with absorption of Ca $(OH)_2$ leading to the formation of calcium silicate hydrate (C-S-H) [4]. Most SCM material, having the ability to activate these cementitious properties are describe as a pozzolan [5]. Calcium hydroxide is the product of first hydration of cement paste leading to development of concrete strength which are often depleted through leaching if the concrete is dominated with pores. The use of Ground Granular Blast-furnace Slag (GGBS) as a cement replacement has shown its viability both as a cementitious material as well as a pozzolan [6–8] in addition to its low carbon footprint. The embodied carbon coefficient of GGBS have been determined using life cycle analysis to be $0.07kgCO_2ekg/m^3$ compared to cement of $0.912kgCO_2ekg/m^3$ [9]. Notwithstanding the low carbon impact of carbon, the development of compressive strength for GGBS when used as a partial cement replacement is slow due to the weak binding effect with cement resulting to poor hydration, microstructure pore generation and slow compressive strength development [10]. However, mitigating these shortcomings associated with the strength development of GGBS when used as cement replacement requires the activation of its cementitious and pozzolanic properties in an alkaline environment. Similar studies have shown satisfying performance in mechanical properties of GGBS based concrete when used as a composite binder [11]. The development of green concrete therefore requires the replacement of calcium oxide inherent in OPC through the activation of SCMs obtained from recycled waste having relatively environmental impact and high structural performance. Owing to the poor strength development associated with GGBS, the introduction of nano silica enables the enhancement of the mechanical properties of green concrete with age. The addition of nano silica resulted to dissolution of hydration products such as calcium hydrates and increases in average chain length of silicates thereby reducing the propagation of porosity in the cement paste which results to improvement in the rate of calcium hydroxide leaching [12]. When GGBS is used as SCM, there are limitation to the extent of percent replacement, as many literatures have reported a decline in mechanical properties for greater than 40% replacement [13–16]. However, this decrease in mechanical performance as the percent replacement increases is also traceable to poor workability of GGBS based concrete due to its high-water absorption [17,18]. The need to increase the percentage cement replacement attract the consideration of concrete geo-polymerization. With the issue of sustainability due to the prevalence of calcium hydrates in Ordinary Portland Cement (OPC) paste exhibiting concerns of anthropogenic emission, geopolymer concrete seeks to replace the calcium oxide responsible for strength development in OPC concrete with aluminium silicate. Regarding the issue of workability, it has been suggested that the addition of superplasticizer improves the workability of concrete which allows for reduction of water in concrete [19].

1.1. Lightweight concrete

The production of light weight aggregate in pellets was developed by the building research Establishment (BRE) in 1950 to produce Pulverised Fuel Ash (PFA) sintered aggregate known as Lytag. The process involved the use of unburned coke in its bulk homogenised form mixed with water fed unto a revolving dish and compacted to about 12–14 mm in sizes before being transferred to an ignition hood for combustion. The moisture is allowed to evaporate through the open nature of finished particles [20]. The sintering of PFA at about 1200–1300°c resulted to the production of light weight aggregate with a chemically inert pellets of a spherical shape often known as Lytag. It is graded as both fine and coarse aggregate. The use of light weight aggregate enhances the reduction of the dead load of the structure with the advantage of promoting longer clear span. The increase in the buoyancy of the lightweight aggregate concrete has been observed with a reduction in the density when submerged to about 55% less of the normal weight concrete with added advantage for use in offshore and marine structures [21]. However, loss in prestress due to higher creep, greater deflection due to poor modulus of elasticity and poor sound absorption have been identified as some of the short comings of lightweight concrete [22]. Concrete density contributes significantly to the development of compressive strength through its influence in predicting the elastic modulus of concrete. With a density of 2400 kg/m^3 for normal aggregate concrete, the determination of load factor on a structure through the structure self-weight can be troubling. To reduce safety and cost effect on a structure and very recently the phenomenon of Alkali Silica Reaction (ASR) associated with normal weight aggregate inhibited by the reaction of hydroxyl ion with reactive silica in the aggregate, the filler ingredient for coarse aggregate, to produce green concrete has attracted many attentions for a shift to light weight aggregate [23]. Light weight aggregate concrete is made from recycled industrial waste. For high density light weight concrete, a density of 1350–1850 kg/m^3 is recommended [24]. This offers the advantage of reduction in reinforcement [25], acoustic performance [26] thermal performance, good flexural strength and long span construction [27]. Amongst other light weight aggregate, Lytag is considered a high strength lightweight aggregate considering its production from the pellets of PFA in combination with bentonite and water sintered at a temperature of 1300^0 C. Due to mineralogy of Lytag, attributes of pozzolanic activities have been suggested [28]. The unreactive properties of silica contained in Lytag have been reported with the structural performance influenced by the porosity as well as the water absorption, hence it is recommended that a pre-soaking for up 24hrs is necessary prior to use in concrete mix [29]. Similar studies showed water absorption for Lytag at 30 min to 15% and 24hrs to be 18%. Decline in compressive strength and workability of concrete was observed with increased dosage of Lytag when optimization of Lytag at different dosage was carried out [30].

1.2. Geopolymer concrete

Polymerization occurs when the chemical combination of smaller molecules forms large chainlike structure catalysed the molarity of the hydroxyl ion are accompanied usually by high temperature. This was observed when sodium hydroxyl ion is combined with sodium silicate to form an alkaline, a heat dissipation of 85^0 C is noted at 15 M sodium hydroxide solution. Supplementary Cementitious Material behaviour in alkaline solution have shown to exhibit improvement in its pozzolanic properties [31]. The morphology of polymers defined by the time of polymerization is a factor that defines the performance of the polymers. In the study of the factors that affect the molecular imprinting procedure demonstrated that prolonged polymerization reaction induces leftovers of unpolymerized molecules causing coagulation and poor mix uniformity [32]. When alkaline solution was left at room temperature for more than two days, the solution coagulates with the crystals of sodium silicate on the walls of the container leaving the aqueous sodium hydroxide solution. The sodium hydroxide solution filtered from the coagulated sodium silicate, when used in concrete is observed to negatively affected the compressive strength of concrete. Aside the benefit of reducing embodied carbon that alkaline activated concrete or geopolymer concrete offers, other outstanding advantages includes enhancing effective thermal insulation properties of concrete, high temperature resistance [33]. The compressive strength of geopolymer concrete have been concluded to significantly depend on the molarity of sodium hydroxide solution [34–36]. The search for alternative solution to cement in producing green concrete, challenges are encountered both with the proposed recycled binder as well as the lightweight aggregate. For example, GGBS is known for poor strength development, poor workability and porosity which subsequently affect the structural performance of the concrete. Regarding the use of lightweight aggregate, porosity has been noted to be responsible for poor strength development. During hydration, the eventual poor strength development is traceable to the leaching of calcium hydroxide which when preserved culminated to the formation of calcium silicate hydrate, which determines the structural performance of concrete. Owing to the need to reduce the carbon content of the normal concrete with OPC as its binder, the activation of GGBS using sodium hydroxide and sodium silicate as alkaline binder increases hydration activation [37]. This activation process in an alkaline environment known as concrete geo-polymerization also aims to replace the diminishing calcium oxide in green concrete with aluminium silicate owing to its replacement with alternative binders. Notwithstanding the alkaline activator, the concept of geo-polymerization assumes credibility when the materials are amorphous and containing reactive aluminium and silica monomers with very low water demand. Available alkaline activators include potassium silicate (K_2SiO_3), sodium hydroxide (NaOH), sodium silicate (Na_2SiO_3) and potassium hydroxide (KOH) [38]. However, studies have shown an increase in activities of the monomers when activated with sodium hydroxide compared to potassium hydroxide [37,39]. With the high-water demand of geopolymer concrete, excessive leaching of early hydration product is eliminated thereby preserving strength development as well as formation of a densified binder paste matrix structure. While this situation will lead to increase in compressive strength, there is the challenge of poor workability which is evident on poor result from slump test. The scarcity of available knowledge on the viability GGBS at high percent cement replacement up to 80% with Lytag inform the need for this study. This offers the advantage of a sustainable green concrete in a geopolymer, based on the pozzolanic activities of Lytag and the low carbon factor of GGBS.

1.3. Significance of study

Review of current work with the use of GGBS as partial replacement of cement for lightweight concrete shows poor strength development, poor workability, and eventual poor compressive strength. The extent of this deterioration is somewhat determined by the percent cement replacement as well as the type of lightweight aggregate used and the mineralogy of the SCM.

The need to replace OPC in concrete implies that CaO which is the strength development mechanism requires replacement with Aluminium oxide. Due to low reactivity of aluminosilicate materials, the use of an activator in an alkaline environment is introduced. The product of the process is a geopolymer concrete which have been noted for low carbon emission, with the mechanical properties optimised using nano silica. Embodied carbon analysis of GGBS shows a low embodied carbon coefficient, hence the need for optimization of its potency for the benefits of sustainability. While the benefits of Lytag as a lightweight aggregate offers the benefit of reduced embodied carbon through low self-weight, reduced reinforcement, long span construction and acoustic performance. The combination of GGBS and Lytag results to the formation of green concrete. To mitigate the impending challenges, the use of silica fume which is nano materials improves the pozzolanic reaction activities in concrete for high structural performance while superplasticizer in an alkaline environment offers enhancement of workability, high strength development, low carbon, and high structural performance in the production of green concrete. This paper aims to develop a novel concrete mix design using lytag to produce a lightweight aggregate low carbon concrete for sustainable design of structures.

2. Materials and methodology

2.1. Materials

The binder materials used in this study were CEMII Ordinary Portland cement 42.5 R (Dragon Alfa,UK) and Ground Granulated Blast-Furnace Slag (Conserv Ltd, UK). CEM II used conforms to BS EN 197 [40] and GGBS conforms to BS EN 15167–1:2006 [41] with density of approximately 2.4–3 g/cm^3(20^0 C). Oxide composition of the binder tested to BS EN 15167–1:2006 are given in Table 1. Densified silica fume Microsilica, Pozzolan, GFRC, 90% (Liquid latex direct, UK) was used as an additive and superplasticizer (Flowaid SCC, UK) as a high-water reducing agent. The materials for preparation of alkaline solution were sodium hydroxide, NaOH DRYI29–1000 (Soap Kitchen Ltd, UK) and sodium Silicate, Na_2SiO_3(Inoxia Ltd, UK). The sodium silicate solution is made of density of 1.30–1.60 kg/L with pH value of 11–13, % w/w=20–60 and molar ratio >1.6;<2.6. The sodium hydroxide pellets contain Sodium Carbonate (Na_2CO_3), %w/w 20.8 max, Sodium Chloride (NaCl), %w/w 0.1 Max, Iron, Fe, ppm 50 Max and NaOH, %w/w 199.0 Min.

Lytag 4/14 mm (Lytag ltd, UK) and ordinary sand were used as the aggregate and conforms to BS EN 933 [42]. The Oxide compositions of the Lytag aggregate is given in Table 2 and the physical properties in Table 3. Fig. 1 Shows particle size distribution of Lytag and sand.

Lytag 4/14 mm is used as the lightweight aggregate to reduce the concrete density and sand is used for the fine aggregate. Using 4 mm and 14 mm sieves for the lightweight aggregates, Lytag has a percentage passing of 9.7–98% respectively. That of sand uses 0.15 mm and 2.36 mm and the percent passing are 0.93–97.23%. The loose bulk density and particle density for Lytag were 8.2 $\times 10^{-7}$ kg/m^3 and 1.42 $\times 10^{-6}$ kg/m^3. The specific gravity of granite used as the normal weight aggregate is obtained as 2.62 and that of the sand is 2.52.

2.2. Preparation of specimen

The specimen was prepared using lytag as its coarse aggregate and locally available natural sand as fine aggregate. Sodium hydroxide and sodium silicate are used as Alkaline activator to improve the mechanical properties of the mixture. Silica fume is added to the binder at 5% of the binder weight and Superplasticizers at a dosage of 1% of the binder weight. Based on reports from available studies that geopolymer concrete performance improves with increases in molarity of the NaOH

Table 1
Oxide composition of GGBS and CEMII (wt%).

	SiO_2	Al_2O_3	Fe_2O_3	CaO	MgO	SO_3	CI	LI	F
CEMII	21.9	6.9	3	63	2.5	1.7			370
GGBS	36.73	12.2	0.58	37.84	9.0	0.1	0.03	1.1	504

Table 2
Oxide composition of Lytag aggregate (wt%).

SiO_2	TiO_2	Al_2O_3	Fe_2O_3	Mn_2O_4	MgO	SO_3	CaO	Na_2O	K_2O
53.6	1.0	26.72	8.57	0.08	1.55	0.03	2.09	1.24	3.65

Table 3
Physical Properties of Lytag(wt%).

pH value	Loss on Ignition (%)	Thermal conductivity, (W/m.k)	Thermal Resistivity (^oC.m/W)	Resistance to Thermal Shock	Plasticity index	Water absorption %
9.3	2.0	0.206	4.87	0.1	Non-Plastic	14.77

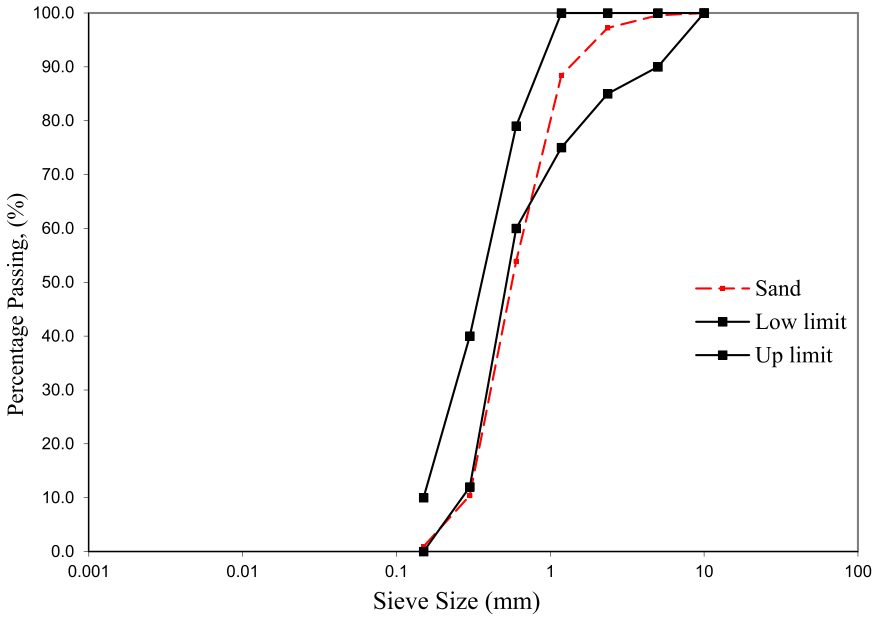

Fig. 1. Particle size distribution of fine aggregate.

solution up to 15 M [31,43–46], the Alkaline activator was prepared at a molarity 15 M using sodium hydroxide (NaOH) solution with sodium silicate (Na_2SiO_3) solution at a Na_2SiO_3/ NaOH ratio of 2.5. The ratio of 1.5–2.5 have been established from previous study to be optimal [47]. Sample constituent's materials for alkaline solution are shown in Fig. 2.

522 g of sodium hydroxide pellet were added to 1 litre of distilled water to produce 15 M solution and mix with sodium silicate solution at a Na_2SiO_3/ NaOH) ratio of 2.5.

2.3. Mix design

The mix design of lightweight concrete according to BS EN 206–1 [48] recommends the use of oven-dried density of 800 kg/m^3 to 2000 kg/m^3 for partially or wholly replacement of dense natural aggregate from a desired density class as presented in Table 4. Based on a density class of 1.8 with slump class S3 and using empirical design chart for Lytag aggregate from the study of Swamy and Lambert [49] and Building Research Station, UK, the concrete mix design was carried out. The process to achieving concrete sustainability aims to transform from the conventional concrete to the green concrete solution using the framework demonstrated in Fig. 3.

Using the strength and properties of lightweight concrete as recommended by Eurocode 2 [50], design mix of four classes of concrete from Table 5 was carried out. The concrete grade is LC20/22, LC30/33, LC40/44 and L50/55. For L20/22; 20 represent 28-day compressive strength from cylinder mould of 20 MPa while the 28-day compressive strength from cube mould is 22 MPa. The steps for concrete mix design are illustrated in Fig. 4. It commences with the choice of density class through the process of determining design strength, water to cement ratio, cement content and ends with concrete constituent materials dry batch. The choice of density class of lightweight concrete is based on the target design strength of concrete.

2.4. Casting and curing of Sample

Lytag was pre-soaked for 24 hours prior to mixing and kept at normal

Fig. 2. (a-d): Selected materials used for concrete mix of the geopolymer concrete specimen.

Table 4
Lightweight concrete density class [50].

Density class	1.0	1.2	1.4	1.6	1.8	2.0
Range of density (kg/m^3)	801–1000	1001–1200	1201–1400	1401–1600	1601–1800	1800–2000
Nominal design density(kg/m^3): Plain concrete	1050	1250	1450	1650	1850	2050

room temperature.

Alkaline solution was prepared at Na_2SiO_3/ NaOH ratio of 2.5 and added to the concrete mix at A/B ratio varied between 0.3 and 0.6 while percent replacement for cement with GGBS varied from 60% to 80%. Superplasticizer was added to the alkaline solution and stir for about 3 minutes while silicate fume at 5% binder weight was added to cement and GGBS and stir for 2 minutes. The combination of GGBS, silica fume, cement and superplasticizer resulted to the formation of Green Concrete Binder (GCB). The sequence of property optimization is shown in Fig. 5. When slump was deficient, free water were added to the mix. After which the Lytag and alkaline solution was added and stir for about 5 mins to obtain the desired green concrete as shown in Fig. 6. The test samples were then place in the mould and wrapped in cling film to prevent loss of moisture. Demoulding was carried out after 24hrs and place in curing tank for 7 and 28days before testing.

2.5. Oven dried density

Structural lightweight concrete is design to meet the equilibrium density requirement with regards to proportioning, finishing and placement. Where consideration is given to fresh density concrete, reduction of concrete density can be achieved using air entrainment to a very demanding value, however there are tendencies for delamination and concrete blisters. It has been observed that density of lightweight concrete attains equilibrium with the environment at a value of 50–130 kg/m^3 less than the fresh density. In determining the oven dried density for lightweight concrete with procedures recommended by ASTM C567 [51], direct measurement requires 90 days for most lightweight concrete and 180 days for high strength lightweight concrete to achieve the required equilibrium for 0.5% weight gain or loss with the sample in a controlled environment. Owing to lengthy day, necessary for direct laboratory measurement, a calculation method is recommended

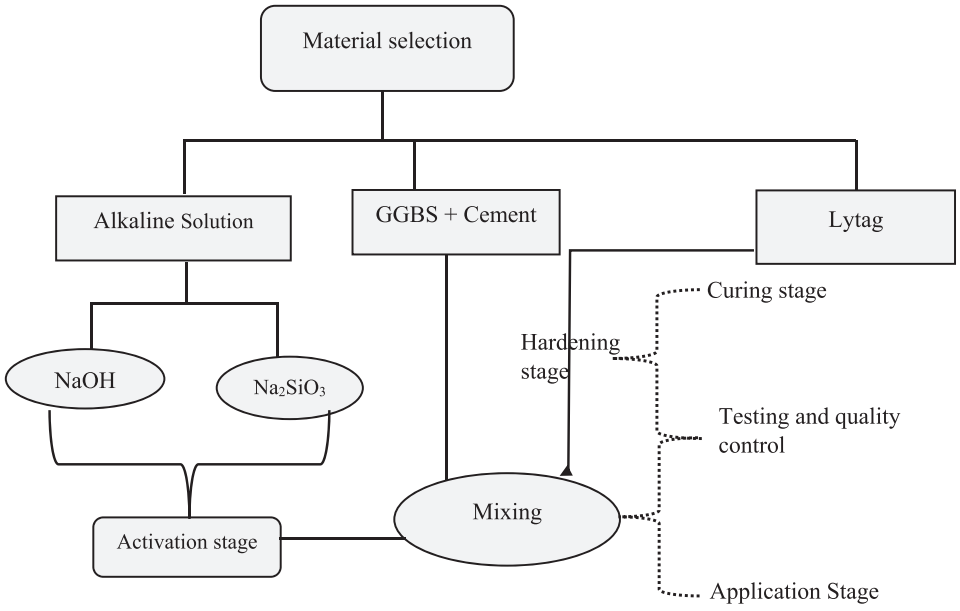

Fig. 3. Development of geopolymer concrete.

Table 5
Lightweight concrete strength classes [50].

	Fck,cy											
	16	20	25	30	35	40	45	50	55	60	70	80
Fck,cube (MPa)	18	22	28	33	38	44	50	55	60	66	77	88
ht, flcm (MPa)	22	28	33	38	43	48	53	58	63	68	78	88

Fck,cube=28 day cylinder compressive strength, ht, flcm=28 day cube compressive strength

in note 1 of ASTM C567 [51] based on the relationship between equilibrium density and oven dried density.

Hence oven dried density O_C is calculated as

$$O_C = \left(M_{df} + M_{dC} + 1.2M_{Ct}\right)/v \quad (1)$$

$$\rho_E = O_c + 50kg/m^3 \quad (2)$$

where M_{df} =mass of dry fine aggregate in the concrete batch; M_{dC} = mass of dry coarse aggregate in the concrete batch, M_{Ct} = mass of cement in the concrete(binder) in the concrete batch, v = volume of concrete produced by the batch, ρ_E = Calculated equilibrium density, O_C = Oven dried density.

The fresh density of the concrete is the summation of all mixture component as an average of the total volume of concrete. The basis of acceptance is such that the fresh concrete density in the field should satisfy the conditions of calculated fresh density ± 50 (kg/m^3) [51].

2.6. Concrete testing

2.6.1. Compressive strength

Using the standards BS EN 12390 [52], the compressive test was conducted on 100 ×100 ×100 mm cube sample in Matest compressive testing machine at a loading rate of 3 kN/sec and a start load of 10 kN. The equivalent cylindrical compressive strength was extrapolated with a factor of 0.8 for Normal weight concrete and 0.9 for lightweight concrete based on the relationship as established by Eurocode 2[49] and presented in Table 5. Modulus of Elasticity, E_c in GPa is obtained using the relation given by Eurocode 2[50] as shown in Eq. 3.

$$E_c = 22\left(\frac{fc}{10}\right)^{0.3}\left(\frac{\rho}{2200}\right)^2 \quad (3)$$

where ρ is the oven dried density of the concrete, fc is the compressive strength of the concrete in MPa. The test set up for compressive strength is shown in Fig. 7.

One hundred and twenty (120) concrete cubes of 100 ×100 ×100 mm were prepared for compressive strength testing, out of which Forty-eight (48) were for the control samples. Two set of control samples were made, with Control A made of lightweight aggregate (Lytag), 100% cement without GGBS and alkaline solution but with the addition of Silica fume at 5% binder and superplasticizer at 1% binder. Control B was made from normal weight aggregate (granite), 100% cement without GGBS, silica fume, superplasticizer, and alkaline solution. Forty (40) specimens were prepared for the flexural test for rectangular beam of 100 ×100×500 mm. The concrete sample were covered after moulding and demoulded after 24hrs to commence curing in the laboratory curing tank for 7 and 28 days at a controlled temperature of 25 °C to ensure that moisture content is maintained. The concrete mix compositions are shown in Table 7. The compressive strength test set up is shown in Fig. 7.

2.6.2. Flexural test

The flexural test was conducted on 100 ×100×500 mm beam sample according to ASTM C293 [53] and BS EN 12390 [54] on Norton machine at a set speed of 5KN/min and a sampling rate of 5 Hz. The flexural strength was determined on the Modulus of Rupture, M_R giving by the relation as stated in Eq. 4.

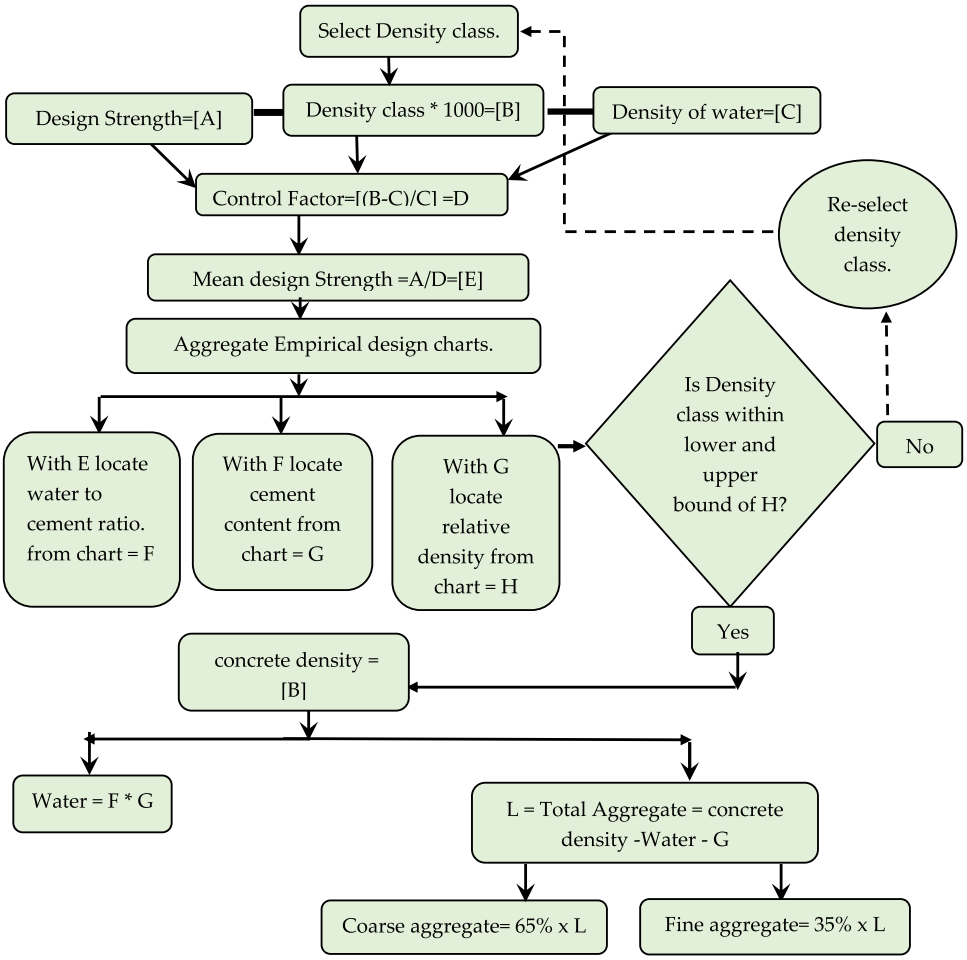

Fig. 4. Mix design procedure for Lightweight concrete.

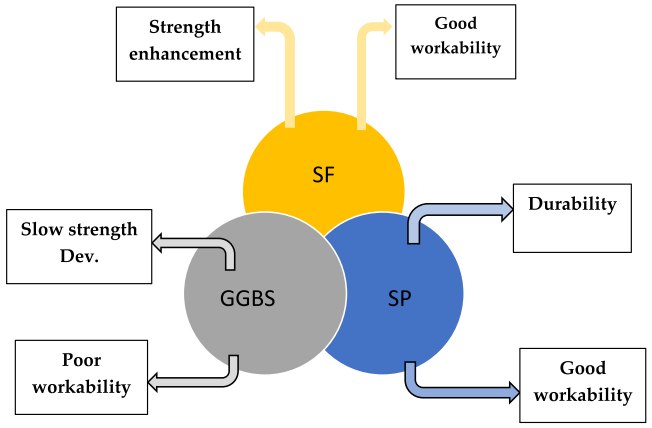

Fig. 5. Preparation of green concrete binder (GCB).

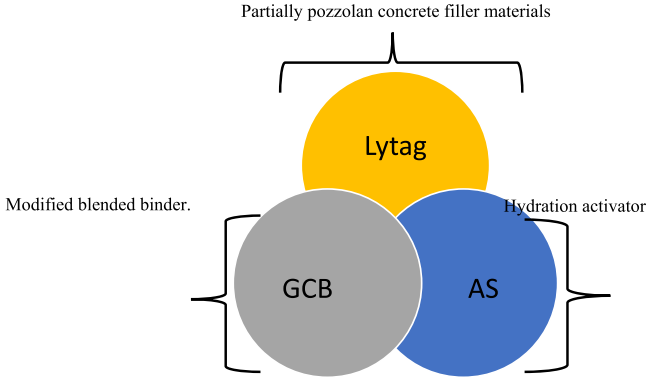

Fig. 6. Mix constituent for Green Concrete (GC).

$$M_R = \frac{PL}{bd^2}(\text{MPa}) \quad (4)$$

Where P is the failure load, L is the beam span between supports, b is the width of the sample, and d is the depth of the sample.

From previous study, the tensile strength of geopolymer concrete have been shown to be related to the compressive strength. This relationship is expressed in Nguyen et al. [55] as:

$$f_{ct} = 0{\cdot}858 fcm^{0{\cdot}410} \quad (5)$$

where f_{ct} is the tensile strength (MPa) and *fcm* is the compressive strength (MPa).

Some selected samples with their broken pieces were subjected to scanning electron microscopy (SEM) to examine microstructural characteristics. The flexural strength test set up is shown in Fig. 8.

2.6.3. *Workability*

For each mix of concrete specimen workability was measured before placing concrete in the mould. Slump test was carried out as specified in BS EN 12350–2 [56]. The measured slumps are presented in Table 6 and the measured value falls within the range of 50–80 mm as shown in

a. Samples for compressive test *b. Sample under compressive test.*

Fig. 7. (a-b): Compressive test set up and concrete sample.

a. Sample under flexural test *b. Sample failure under flexural test*

c. Set of Beam sample *d. Sample failure under flexural*

Fig. 8. (a-d): Flexural test of sample.

Fig. 9. The concrete mix proportion is as shown in Table 7.

2.7. Stress Strain relation

The result of the compressive test is presented in Figs. 10–11 using mathematical function derived by Zhou and Wu [57] using Eq. 6 to characterize and establish the stress strain relationship of the concrete using the compressive strength.

$$f(x) = \frac{4fm}{(1+C)^2}\left[e^{-\frac{x}{xo}\ln\left(\frac{2}{1-C}\right)} + C\right]\left[1 - e^{-\frac{x}{xo}\ln\left(\frac{2}{1-C}\right)}\right] \quad (6)$$

where C is a factor that depend on the internal friction of the concrete define by the poison ratio, x is the compressive strain, xo is the

Table 6
Workability (slump).

Concrete Specimen	Slump (mm)
LC20	64
LC30	63
LC40	65
LC50	72
NWC20	70
NWC30	73
NWC40	75
NWC 50	55
LC20/60	60
LC20/70	54
LC20/80	60
LC30/60	63
LC30/70	66
LC30/80	58
LC40/60	59
LC40/70	61
LC40/80	65
LC50/60	63
LC50/70	56
LC50/80	64

a: Concrete slump LC20/60 *b: Concrete slump LC20/80*

Fig. 9. Slump test of concrete sample.

maximum compressive strain (‰), fm is the maximum compressive stress and f(x) is compressive stress (MPa). The value of C= 0.15 is used in this study as determined and used to model shape of the stress strain curve [58]. The modulus of Elasticity, E is derived from the relation as stated in Eq. 3. The point (fm, xo) is the local minimum point that defines the point of maximum compressive stress and compressive strain, where x is the compressive strain.

3. Results and discussion

3.1. Compressive strength

The compressive strength of the specimen is presented in Table 8 and Figs. 10, 11, 12, 13 and 14 shows the compressive strength of the concrete specimen for all mix. The compressive strength as shown in Table 8 is an average of 3 concrete specimen tested at 7 and 28 days. The standard deviation across the samples for 7 day strength varies between 0 and 2.39 MPa. However, a standard deviation of 6.36 MPa was observed with the LC40 sample. This implies that the value deviate from the average with 6.49 under 7 days of strength development and could be liken to poor hydration. Increase in compressive strength from 30.40 MPa to 35.00 MPa for LC20/60 is observed as cement replacement with GGBS increased from 60% to 80%. This is due to hydration activity enhanced with the alkaline solution which led to changes in the w/c ratio. Maximum compressive strength is noted for LC20/80 at 35 MPa for w/c of 0.77 compared with LC20/60 for w/c ratio of 0.38. This result agrees with previous studies that high water absorption is associated with lightweight concrete and could improve mechanical performance [18,58,59]. The behaviour of the geopolymer concrete is likened to resistance in aggregate disintegration by weathering and freeze-thaw cycles which is linked to the viability of the A/B ratio. In measuring the performance of geopolymer concrete with regards to A/B ratio, Soundness test from literatures indicate that cementitious activity of geopolymer concrete suggest higher A/B ratio for optimal performance in GGBS based polymer concrete [60–62]. The increase in GGBS composition from 60% to 80% resulted to additional free water to attain workability which enhances high compressive strength. With the high SiO_2 composition of 36.73% in GGBS compared to OPC of 21.9%, makes GGBS to exhibit more pozzolanic activity and place more demand in water for effective hydration. High water absorption of Lytag aggregate contributed to the water demand which enhances the densification of paste matrix structure. For LC30/60, compressive strength is maximum at 43.59 MPa compared to LC30/70 and LC30/80. It is noteworthy that there was no free water needed to attain workability, hence the increase in A/B to 0.6. That of LC30/70 and LC30/80 were kept at A/B ratio of 0.3 with added free water to attain workability. Increases in alkali concentrations due to increase in the A/B ratio is noted to improve compressive strength of geopolymer concrete [63]. This implies that more Alkaline Silicate Gel (ASG) were activated, and a more densified matrix of the specimen formed. Some microcracks were noted to propagate though not deleterious as strength was not impeded. The high silica content of GGBS compared to OPC fertilizes the environment needed for geo-polymerization using the available alkaline activators. Geo-polymerization process inhibits high water demand when used in combination with silica fume and superplasticizer [64]. Previous study conducted using capillary suction experiments shows that GGBS exhibited 18% water absorption when used as cement replacement [65]. A reduction in compressive strength is accompanied with increase in A/B ratio to 0.6 for LC40/80. Also, an increase in compressive strength was noted for LC40/70 specimen at A/B ratio of 0.5. This can be attributed to the influence of A/B in improving the mechanical performance of geopolymer concrete without the addition of free water. The ability of superplasticizer to reduce porosity and enhance concrete mechanical properties has been established from previous study [66]. Across the entire specimen, increase in A/B ratio resulted to additional free water which is noted to enhance the concrete mechanical properties. However, a decline in result is noted with 80% GGBS with an associated increase in A/B ratio. Fig. 10 shows that LC20 specimen for the control A recorded 81.48% of the 28-day compressive strength within 7 days of age. This can be attributed to the influence of silica fume on lightweight concrete owing to its fineness and pozzolanic properties compared to the normal weight concrete [67]. This reaction leads to the formation of Calcium Silicate Hydrate (CSH), which is responsible for the improvement in concrete compressive strength [68]. With the trend in compressive strength and A/B ratio as shown in Fig. 11, it is safe to suggest that optimal hydration of GGBS based concrete occur at the glass transition point occasioned by a threshold in A/B ratio and aided with the activities of silica fume [69]. The compressive strain of the concrete specimen is presented in Table 8 with standard deviation ranging from 0 to 0.2 ‰. The Compressive strain for the geopolymer concrete is maximum at 60% GGBS for LC50 as shown in Table 10 and Fig. 15. It can be deduced that the addition of silica fume to geopolymer concrete decreases porosity and enhances ultimate compressive strain as the concrete densification can be likened to reduced porosity [70]. The use of compressive strain for the development of concrete design equation, using the stress block analysis, shows that high ultimate compressive strain increases the moment of resistance of the concrete [25]. It also provides the parameters to describes concrete fracture behaviour based on the softening branch using concrete constitutive model. The error bars on the concrete specimen shown in Fig. 14 indicates the standard deviation, which implies that higher variability is associated with the longer bar when considering a particular concrete type in the specimen. With regards to the deviation of individual specimen from the average, greater variability is seen as

Table 7
Concrete mix composition.

Concrete Mix	CEMII (Kg/m^3)	Lytag (Kg/m^3)	Granite (Kg/m^3)	Sand (Kg/m^3)	GGBS (60% binder wt) (Kg/m^3)	GGBS (70% binder wt) (Kg/m^3)	GGBS (80% binder wt) (Kg/m^3)	SF (5% binder wt) (Kg/m^3)	SP Kg/m^3(1% binder wt) (Kg/m^3)	A/B*	w/c
Control A											
LC20	260	812		437				13	2.6	0	0.37
LC30	330	780		420				16	3.3	0	0.18
LC40	475	670		361				24	4.75	0	0.13
LC50	570	608		327				28	5.7	0	0.1
Control B											
NWC20	350		1197	600							0.7
NWC30	370		1184	593							0.65
NWC40	430		1152	576							0.55
NWC50	520		1105	551							0.45
Geopolymer concrete											
LC20/60	104	812		437	156			13	2.6	0.3	0.04**
LC20/70	78	812		437		182		13	2.6	0.3	0.05**
LC20/80	52	812		437			208	13	2.6	0.3	0.08**
LC30/60	132	780		420	198			16	3.3	0.6	-
LC30/70	99	780		420		231		16	3.3	0.3	0.06**
LC30/80	66	780		420			264	16	3.3	0.3	0.06**
LC40/60	190	670		360	285			24	4.75	0.3	0.03**
LC40/70	142	670		360		332		24	4.75	0.5	-
LC40/80	95	670		360			380	24	4.75	0.6	-
LC50/60	228	608		327	342			28	5.7	0.6	0.6**
LC50/70	171	608		327		399		28	5.7	0.5	0.6**
LC50/80	114	608		327			456	28	5.7	0.5	0.6**

Note: Percentage of silica fume is 5% and super plasticiser 1% of the weight of the binder for all concrete specimen except for the control mix B where normal weight aggregate was used. There is additional free water due to workability to the geopolymer concrete sample.
Control A = control mix (100% PC with Lytag aggregate);
Control B = control mix (100% PC with Granite aggregate);
A/B*=alkaline- binder ratio.
SF = silica fume;
SP = superplasticizer
** = water to cement ratio due to free water added

indication of larger standard deviation. A maximum deviation of 5.74 is observed for the 28-day compressive strength as shown in Table 8.

3.2. spearman's ranked correlation coefficient

The use of Pearson's correlation coefficient provides an evaluation for a linear relationship of covariance on two data sets. Spearman rank correlation coefficient was used to compare the correlation coefficients between Superplasticizer to Silica fume ratio (SP/SF) ratio and compressive strength. Due to sensitivity of outliers [71] which is obvious with the disparity of SP/SF ratio as shown in Table 8 and the conditions of data set normality, Spearman's ranked correlation coefficient is recommended for a better statistical correlation [72]. The estimator as proposed by Musarat et al. [72] is shown in Eq. 7:

$$R_s(x_i, Y_i) = 1 - \frac{6\sum_{i=1}^{k} d_i^2}{k\left(k^2 - 1\right)} \tag{7}$$

Where X_i^1 and Y_i^1 are the ranks of X_i and Y_i respectively., $d_i = \left(X_i^1 - Y_i^1\right)$ and k is the number of observations.

Evaluating Table 8 using Eq. 7 shows Pearson's rank coefficient of 0.334. A correlation coefficient of 0.334 suggests a positive relation between SP/SF ratio and compressive strength. It can be deduced that as SP/SF increases, there is a tendency for compressive strength to increase which implies a monotonic relationship. The significance of this correlation was compared with a table of critical values for Spearman's rank correlation coefficient at a specific significance level of 0.05 and a p value of 0.380 was obtained. It can be deduced that there is not enough evidence to conclude a statistically significant relationship between SP/SF and compressive strength since p value is greater than 0.05.

3.3. Effect of free water and A/B ratio

Addition of water to geopolymer concrete has impact on workability as well as structural integrity of the concrete. Such addition is aimed at improving workability and other parameters related to strength enhancement. The relationship between free water and A/B ratio shows that the mechanical performance of the GGBS blended Lytag geopolymer concrete is not influenced significantly by the addition of free water. From the results of influence of superplasticizer to silica fume ratio (SP/SF), as noted in Fig. 16 with maximum compressive stress exhibited by the LC20/80, LC30/60, LC40/70, and LC50/60 samples. On comparing the outcome of LC20 geopolymer concrete, for LC20/60 and LC20/70, with added free water equivalent to w/c of 0.08 and further analysis of influence of superplasticizer to silica fume ratio (SP/SF), indicates that SP/SF ratio contributes sufficiently to the concrete performance. For each concrete specimen of LC20, LC30, LC40 and LC50 for the geopolymer concrete, compressive strength increases with decreasing SP/SF ratio to optimal ratio of 0.2. Findings from literature indicate that additional free water of 20–35 kg/m^3 improves workability to 165% [73], however reduction in the compressive strength was observed. This implies that free water can negatively affect modulus of elasticity of geopolymer concrete. On varying A/B ratio, it was noted that compressive strength increases up to A/B ratio of 0.6 with added free water. This is attributed to SP/SF ratio of 0.17 for LC2080, 0.19 for LC3060 with no added water, 0.19 for LC40//60 with added free water and 0.19 for LC50/60 with added free water. The impact of A/B ratio controls the performance of concrete leading to densification of the binder paste. Fig. 16. shows that increase in A/B ratio resulted to increase in compressive strength, however good performance is noted when A/B and free water were on the same value. The impact of free water could not be attributed to the concrete behaviour as improvement were noted at LC30/60 and LC40/70 with no added free water. Previous study has shown that increasing the solution of NaOH to 14 M, resulted

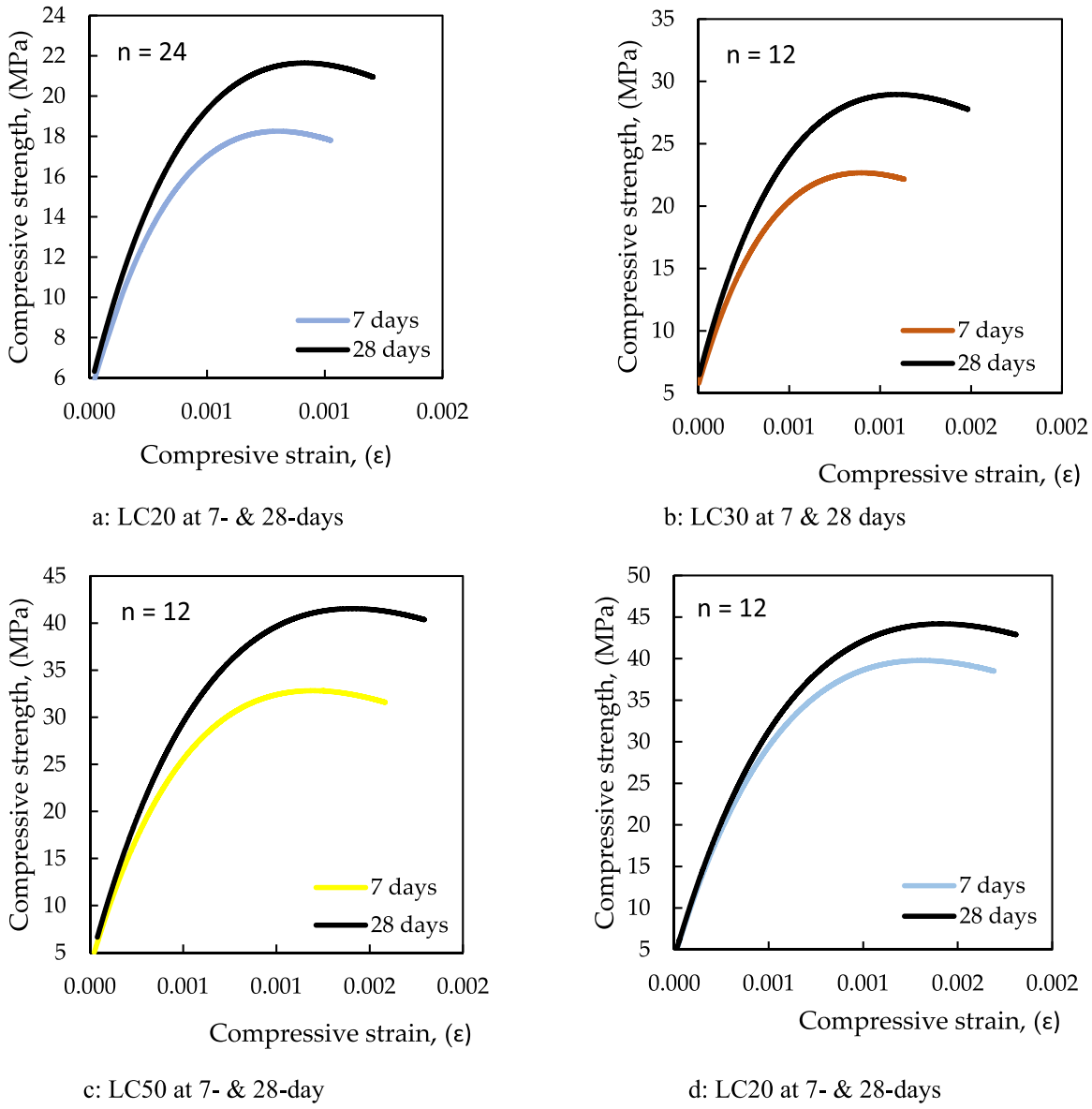

Fig. 10. (a-d): stress-strain behaviour for strength development between 7 and 28 days for Control A sample taken after 7 and 28 days of curing.

to optimal A/B ratio of 3.5 [74]. It is necessary to optimising A/B ratio for the geopolymer concrete as higher ratio could be deleterious to reinforcement in the concrete structure. The alkaline binder which consists of Na_2SiO_3 and NaOH acts as an activator for the aluminosilicate composition in GGBS to form a network of three-dimensional network of aluminosilicate gel, which serves as the binding phase in geopolymer concrete. The formation of the gel influence porosity and pore structure. It also controls the setting, hardening reactions, and the overall micro-structural characteristics of geopolymer concrete. The optimal A/B ratio in this study is observed for LC30/60 at 0.6, LC40/70 at 0.5 and LC50/60 at 0.6.

3.4. *Flexural strength*

Flexural of the concrete specimen are presented in Table 9 and shown in Fig 17 for the lightweight GGBS silica fumed blended geopolymer concrete, control sample A and B. Control B contains normal weight concrete with 100% OPC. Control A contains 100% OPC with 5% silica fume and lytag aggregate. Beam 1 specimen of size 100×100×500 mm consist of 2 beams and was tested after 28 days curing, while that of Beam 2 specimen of size 100×100×500 mm consist of 2 beams and was tested after 7 days curing. From the result, the flexural strength of control A specimen decreases by 15.84% compared to the control B specimen. Increase in flexural strength from 5.28 MPa to 6.078 MPa for the geopolymer concrete as GGBS increases from 60% to 80% was observed, which indicates a growth of 13.13%. Flexural strength development for control A is 36.25% between 7 and 28 days compared to 22.95% for normal weight concrete. Studies have indicated that there is an optimum amount of silica fume that can be added to concrete mixtures to achieve maximum compressive and flexural strength. Typically, an addition of around 10–15% of silica fume was suggested from previous study for optimal performance [75] compared to 5% that is used in this study. Concrete sample, LC20 with 60% GGBS shows flexural strength development between 7 and 28 days of 24.81% while that 80% GGBS shows 13.62%. This is attributed to increase in composition of GGBS in the concrete which resulted to decline in flexural strength. Addition of 2% silica fume to GGBS based geopolymer concrete was shown to improve flexural strength by 6.67% [76].

3.5. *Influence of Oven dried density on low carbon concrete strength*

The density of concrete is considered to significantly determine the

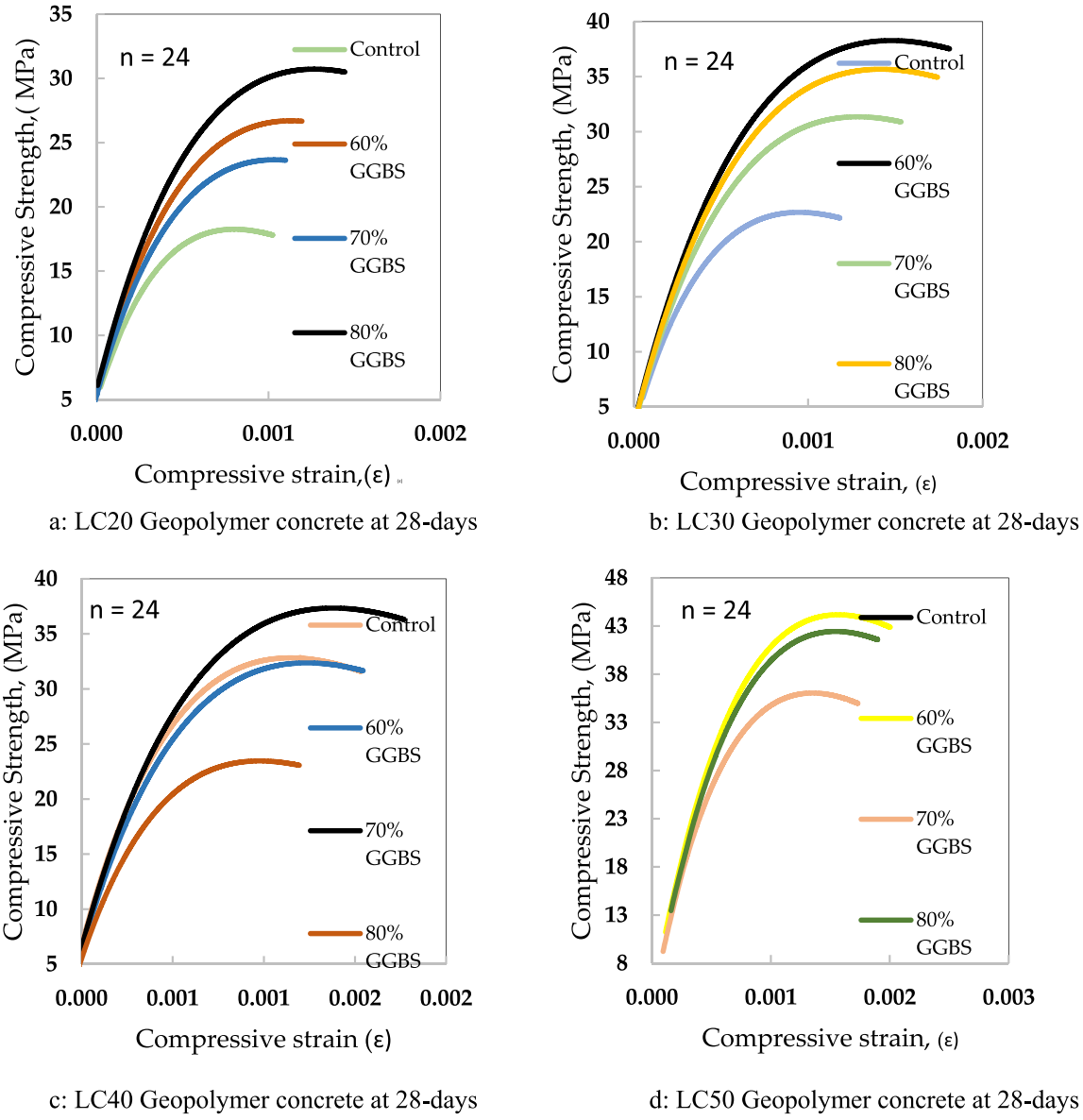

Fig. 11. (a-d): stress-strain behaviour for geopolymer concrete sample taken at 28 days of curing.

behavior of concrete. However, ASTM C567 [51] establishes that there is a reduction in the density of the lightweight concrete as it ages and this reduction continues to such a limiting value known as equilibrium density for which there is no further reduction. The equilibrium density is measured to differ from the oven dried density by 50 kg/m^3. Hence it is recommended that the design of the lightweight concrete be dependent on the oven dried density such that acceptable field density should be limited to calculated fresh density ± 50 kg/m^3. From the result obtained and as shown in Table 10, that after 28 days of concrete curing in water, the lightweight concrete of the control sample (Control A) increases in density by 5% of the oven dried density while that of the geopolymer concrete increases by 10% of the oven dried density. It is noted that while oven dried increases the ultimate compressive strain of the lightweight concrete, the fresh and normal density reduces the compressive strain. The ultimate compressive strain is a fundamental stress block parameter that influence the moment of resistance and eventually determines the viability of the design equation which implies that the higher the ultimate compressive strain, the higher the moment of resistance. From the oven dried density test, it is observed that as the percentage of GGBS increases, there is a reduction in the oven dried density of the concrete, and an increase in ultimate compressive strain. There is no remarkable change in compressive stress due to this change in ultimate compressive strain. Application of w/c ratio on GGBS based polymer concrete was observed to be in the range of 0.37–0.4 with the optimal w/c occurring at 0.37[77]. It can also be observed that the measured concrete density is within the limit as recommended by ASTM C567 [51].

3.6. Embodied carbon

Mitigating the effect of cement on carbon emission after replacement with Supplementary Cementitious materials can be assessed from evaluation and measurement, using the standard defined by Environmental Product Declaration (EPD). A standard methodology for calculating embodied carbon impacts of buildings which is, the amount of carbon emission due to material extraction, manufacturing, transportation of materials to site and construction or installation of materials as recommended using the BS EN15978 [78]. The standard provides the core rules for calculating carbon emission using the EPD for construction product performance indicator in terms of carbon emission for raw

Table 8
Mechanical response of the concrete specimen.

Concrete specimen	Compressive strength (MPa)		SP/SF ratio	Compressive strain(‰)	Standard deviation		
	7d	28d			7d (MPa)	28d (MPa)	Compressive strain (‰)
LC20	20.35	24.66	0.2	1.3	0.42	1.34	0
LC30	25.81	33.11	0.19	1.5	0.00	5.74	0.2
LC40	41.23	47.29	0.20	1.8	6.36	1.60	0
LC50	43.11	50.33	0.19	1.8	2.39	3.02	0.1
NWC20	34.00	34.60	0	1.5	0.47	0.53	0
NWC30	34.63	35.96	0	1.4	1.39	1.39	0
NWC40	39.00	38.52	0	1.7	0.53	0.53	0
NWC 50	34.13	35.36	0	1.9	2.22	2.22	0
LC20/60	22.70	30.40	0.21	1.6	1.25	0.81	0
LC20/70	20.31	26.95	0.19	1.8	0.68	1.49	0.1
LC20/80	30.54	35.00	0.17	1.3	1.65	2.38	0.1
LC30/60	39.87	43.59	0.19	1.8	2.19	2.15	0.1
LC30/70	33.84	35.70	0.20	1.3	2.60	1.81	0.1
LC30/80	36.88	40.60	0.22	2	1.59	0.92	0
LC40/60	34.97	36.92	0.19	1.6	1.53	4.38	0.1
LC4070	33.89	42.51	0.20	1.8	1.45	1.33	0
LC40/80	23.83	26.73	0.19	1.3	1.75	1.99	0.1
LC50/60	33.82	50.30	0.19	2.0	2.35	0.63	0.1
LC50/70	20.35	41.04	0.20	1.7	1.85	1.34	0.1
LC50/80	25.81	48.32	0.19	2.0	0.81	5.74	0.0

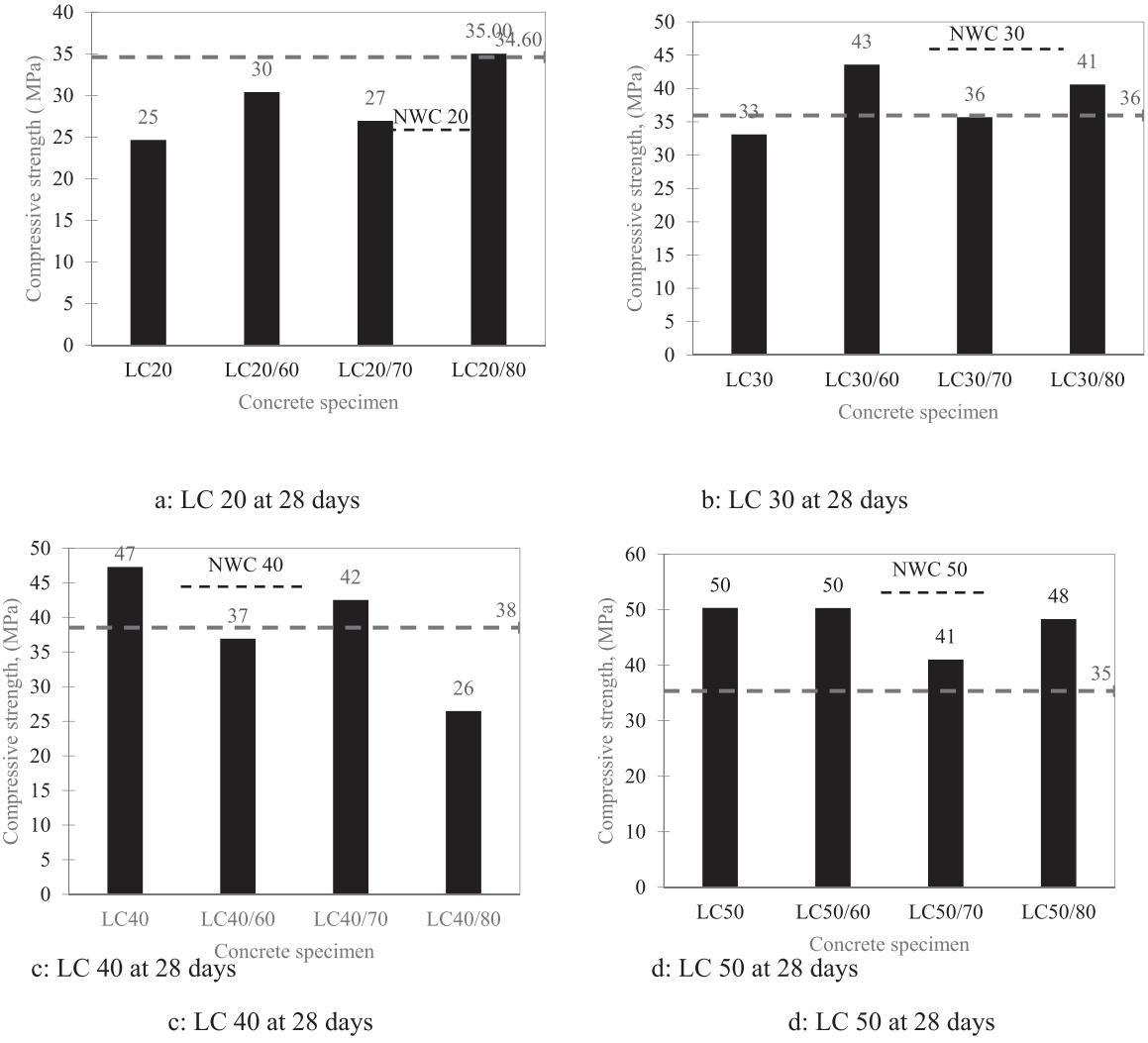

Fig. 13. (a-d): Compressive strength of Lightweight geopolymer concrete sample taken after 28 days of curing showing normal weight concrete as the threshold.

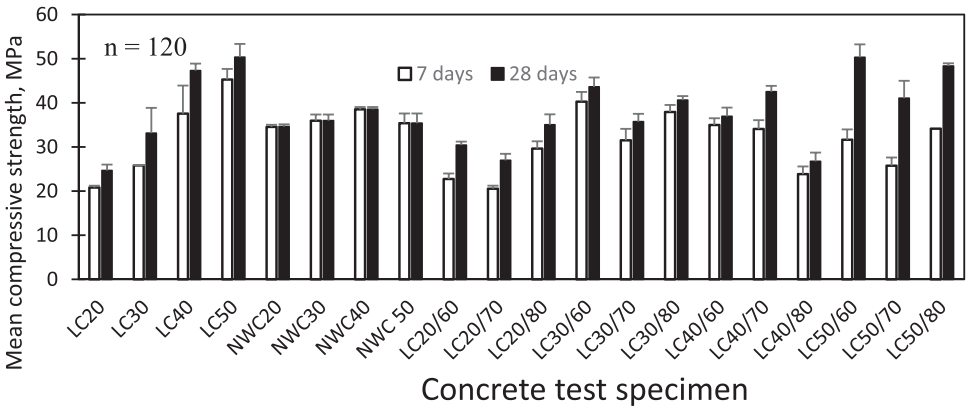

Fig. 12. Compressive strength of concrete specimen sample taken after 28 days of curing with error bars showing standard deviation.

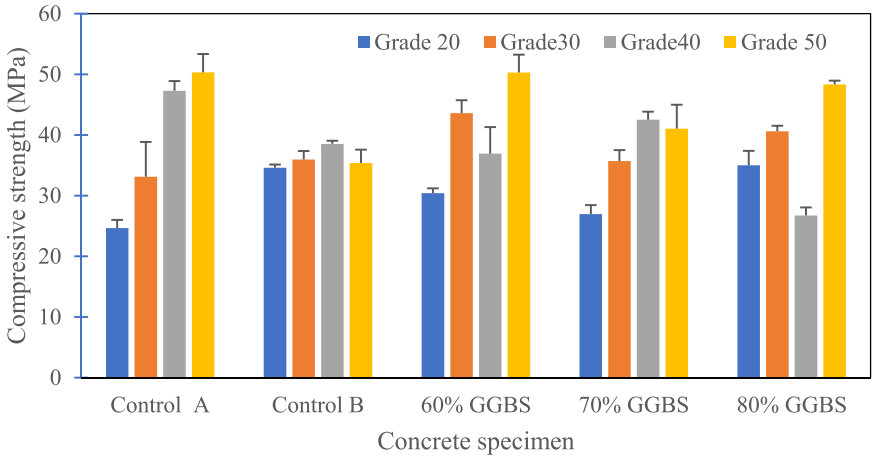

Fig. 14. Comparative Performance of GGBS Silica fume blended geopolymer light weight concrete sample taken after 28 days of curing.

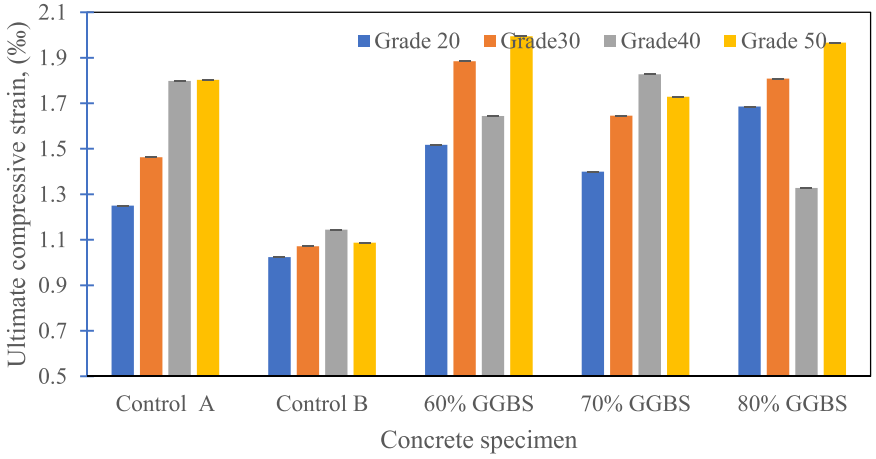

Fig. 15. Compressive strain of GGBS Silica fume blended geopolymer light weight concrete sample taken after 28 days of curing.

materials (A1 emission), transport (A2 emission) and manufacturing (A3 emission). Based on this standard Global Warming Potential (GWP) for embodied carbon is calculated using Eq. 8, with the embodied carbon value as an equivalent of GWP from embodied carbon coefficient ($kgCO_{2e}/kgm^3$) and shown in Table 11.

$$E_{\omega_P} = \sum_{i=1}^{n} sm_{\varnothing i} \times ECC_i \tag{8}$$

Where i= material element in the concrete, sm∅ =concrete materials (kg/m^3), E_{WP}=global warming potentials($kgCO_{2e}/m^3$), ECC_i =embodied carbon coefficient ($kgCO_{2e}/kg$).

Embodied carbon coefficient obtained from literatures for the concrete specimen at the different material composition were used to calculate the associated embodied carbon for the specimen. The calculated embodied carbon as shown in Table 12 suggest evidence of significant reduction when compared to the control B specimen. From

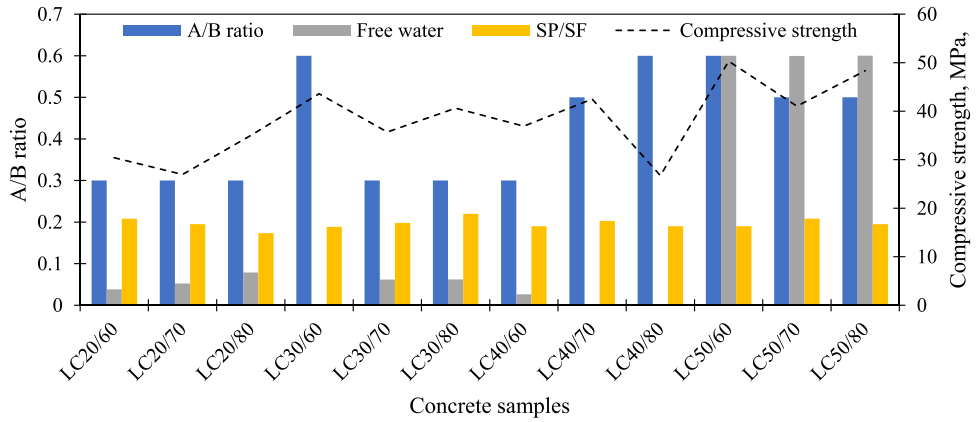

Fig. 16. Influence of free water, A/B ratio and SP/SF ratio on compressive strength of geopolymer after 28 days curing.

Table 9
Flexural testing of the experimental concrete sample for 7 and 28 days of age.

Concrete specimen	Flexural strength at different age (MPa)			
	7 days	7d Standard deviation	28 days	28d standard deviation
Control A	5.97	2.97	9.37	4.65
Control B	7.10	3.52	11.14	5.53
LC20/60	3.97	3.22	5.28	2.62
LC20/70	4.04	2.00	4.67	2.32
LC20/80	5.25	2.61	6.07	3.01
LC30/60	6.13	3.04	6.02	2.99
LC30/70	5.36	2.6	5.27	2.62
LC30/80	5.19	2.58	5.10	2.53
LC40/60	5.54	2.75	5.44	2.7
LC40/70	6.38	3.17	6.27	3.11
LC40/80	4.01	1.99	3.94	1.96
LC50/60	2.17	1.08	4.11	2.04
LC50/70	2.58	1.28	3.96	1.97
LC50/80	1.98	0.99	3.42	1.70

Fig. 18, it is shown that control A reduces embodied carbon emissions in concrete 73.13%. Regarding the grade of concrete, LC20 indicates that a high reduction compared to LC50. This is attributed to volume of cement at the different grade of concrete. With OPC was replaced with GGBS, the reduction increases to 73.23% for 60% GGBS, 75,12% for 70% GGBS and 77.01% for 80% GGBS. The reduction in embodied carbon emissions as shown is attributed to reduction in cement for the concrete and high embodied carbon coefficient of granite compared to Lytag aggregate. The effect of silica fume and superplasticizer in control A has minimal impact on embodied carbon, considering their embodied carbon coefficients. From Tables 12 and 13, there is an indication that, the geopolymer concrete as demonstrated in this study reduces embodied carbon in concrete in the range of 69.19–76.87%.

3.7. Scanning Electron Microscopy (SEM)

Fig. 19 shows the SEM micrograph of the geopolymer concrete specimen. Physical assessment shows propagation of pores and microcracks for the concrete samples This is indicative of poor hydration which does not impede its mechanical performance, as effective hydration was yet to be attained. There was no physical appearance of deleterious substance as SEM analysis on the lightweight geopolymer concrete and shows no trace of ASR phenomenon [82]. Silica and calcium are the two determinants of the mechanical performance of geopolymer concrete as shown in the spectral analysis.

The concrete interfacial zone (ITZ) exists between the cement paste matrix and the aggregate and has have been estimated for normal weight concrete to measure between 50 and 100 μm [83]. Good mechanical behaviour of concrete is likened to a densified bond in interfacial zone. Due to porosity of lightweight aggregate and the tendency for high water absorption, the leakage of water containing silica from the lytag present a no distinct appearance of the interfacial zone densified with the geopolymer cement paste matrix as shown in micrograph of Fig. 20. This indicates that the characteristic of good structural behaviour of the geopolymer concrete is good and well bonded within the interfacial zone. The disparity between the aggregate and cement paste matrix has been described as the wall effect which varies for the normal weight concrete and contributes to poor strength development. This was expressed by Zhang and Gjørv [84] as a phenomenon that described the interlocking force of the lightweight aggregate with the cement paste. The SEM for LC20 at 60% GGBS shows little, or no void within the concrete matrix compared to the LC20 control sample. However, this polarisation of microcracks is predominant within the microstructure which suggest that the added free water, which is equivalent of w/c of

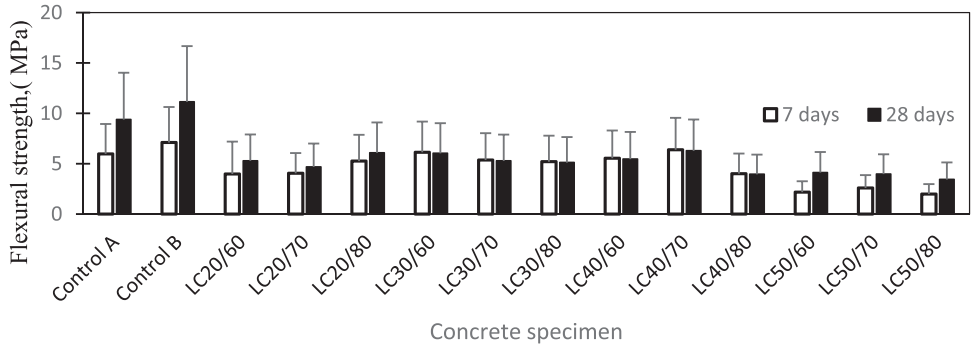

Fig17. Flexural testing of the experimental concrete sample (size 100 ×100×500 mm) taken after 7 and 28 days of curing with error bars showing standard deviation.

Table 10
Concrete specimen oven dried density calculated and measured density after 28 days curing.

Mix	W/c	Oven dried density, (kg/m^3)	Calculated Fresh density, (kg/m^3)	Predicted field density according to ASTM C567 [51] (kg/m^3)	Measured Concrete density after 28days of curing in water. (kg/m^3)	Ultimate compressive strain, (‰)
LC20	0.37	1819	1891	1941	1906	1.3
LC30	0.18	1863	1911	1961	1968	1.5
LC40	0.13	1905	1897	1947	1990	1.8
LC50	0.09	1944	1901	1951	2008	1.8
LC20/60	0.04*	1777	1942	1992	1954	1.5
LC20/70	0.05*	1774	1939	1989	1915	1.4
LC20/80	0.08*	1771	1935	1985	1954	1.7
LC30/60	0.00	1808	1974	2024	2016	1.9
LC30/70	0.06*	1805	1970	2020	1936	1.6
LC30/80	0.06*	1801	1966	2016	1950	1.8
LC40/60	0.03*	1826	1987	2037	2002	1.3
LC40/70	0.0	1821	1982	2032	2090	1.8
LC40/80	0.0	1815	1976	2026	2020	1.3
LC50/60	0.6*	1944	1901	1951	2021	2

* = w/c due to added free water, Predicted field density = calculated fresh density + 50 (kg/m^3)

Table 11
Embodied coefficient for concrete materials.

Concrete Material	Cradle to gate(A1-A3) GWP [kgCO_2ekg/m^3]	Source
GGBS	0.07	[79]
Granite	0.70	[80]
CEM1	0.912	[80]
Sodium Hydroxide	0.86	[80]
Sodium Silicate	0.43	[81]
Lytag	0.249	[80]
River sand	0.005	[80]
Silica fume	0.014	[80]
Superplasticizer	0.01	[81]

0.04, is not sufficient for complete hydration. Spectra analysis as shown Fig. 21 and presented in Table 14 shows that it contained a maximum of 60.54% of Calcium and 17.15% silica. For specimen LC20/70 at 70% GGBS the concrete paste becomes densified and devoid of microcracks. Spectra analysis as shown Fig. 20 and presented in Table 15. shows that it contained a maximum of 21.35% of Calcium and 40.61% silica. Improvement in hydration was noted compared to that of 60% GGBS with added free water.

Formation of hardened substance is observed for LC20 at 80% GGBS as shown in Fig. 18 appears to be Sodium Silicate Hydrate (S-S-H) and reduce propagation of microcracks. This shows that added free water which is equivalent to w/c of 0.05, is sufficient to enhance good

Table 12
Embodied carbon (kgCO_2ekg/m^3).

Concrete specimen	Control B	Control A	60% GGBS	70% GGBS	80% GGBS	Standard deviation (60–80% GGBS)
LC20	1160	442	310	289	267	21.91
LC30	1170	499	333	305	277	27.81
LC40	1201	602	362	322	282	39.93
LC50	1251	673	385	337	289	48.04

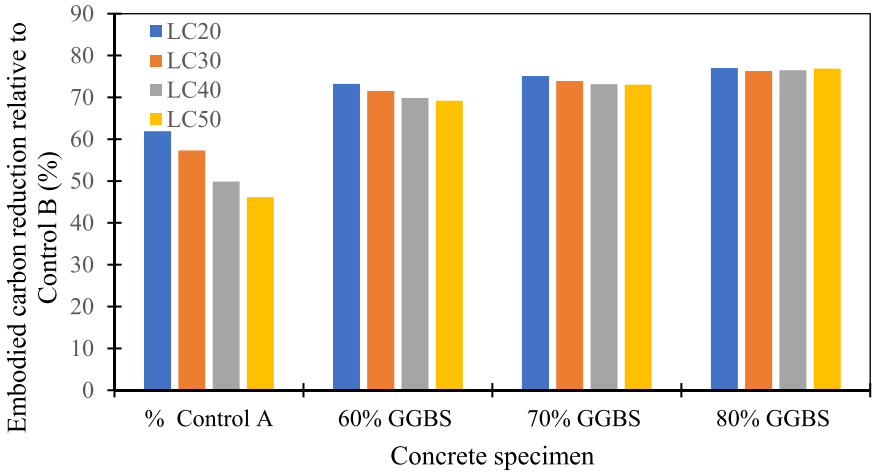

Fig. 18. Embodied carbon for GGBS replacement with cement in Geopolymer concrete.

Table 13
Embodied carbon reduction relative to Control B (%).

Concrete specimen	Control A	60% GGBS	70% GGBS	80% GGBS
LC20	62	73	75	77
LC30	57	71	74	76
LC40	50	70	73	77
LC50	46	70	73	77

hydration with densification of the paste devoid of microcracks with no visible presence of unreacted GGBS. Spectra analysis as shown in Fig. 22 and presented in Table 16 indicate a maximum of 21.95% of Calcium and 45.84% silica. It can also be observed that as the percentage of cement composition reduces due to increase in GGBS replacement, the concrete chemical composition reduces in calcium and increases in silica.

Specimen LC30 at 60% GGBS shows the propagation of microcracks and was randomly distributed within the microstructure. It is obvious, because there is no added free water to complement the A/B ratio of 0.60. Spectra analysis as shown Fig. 23 and presented in Table 17 shows that it contained a maximum of 44.47% of Calcium and 34.15% silica. Notwithstanding the propagation of microcrack due to no added free water, the silica composition compared to LC20 is high which is traceable to increase in compressive strength to 37.53 MPa. Particles of the sample used for the SEM analysis were obtained from remnant of failed sampled under compressive test. The distribution of microcracks as shown in the micrograph of Fig. 19(c-d) could have been formed because of stress field generated when it was under compressive test [85]. The chance of incomplete hydration activity is also suggested as the samples were tested after 7 days of curing. Evidence of a few unreacted GGBS particles as shown in Fig. 19(a-b) and micropores Fig. 19(f) are due to incomplete hydration for LC30 [86]. However, in contrast to slow reactivity and poor hydration, the presence of unreacted particles reduced in LC30/60 as shown 23(c-d) and 24(e-f) and has been reported to be due to the enhancement of the amorphous phase with the addition

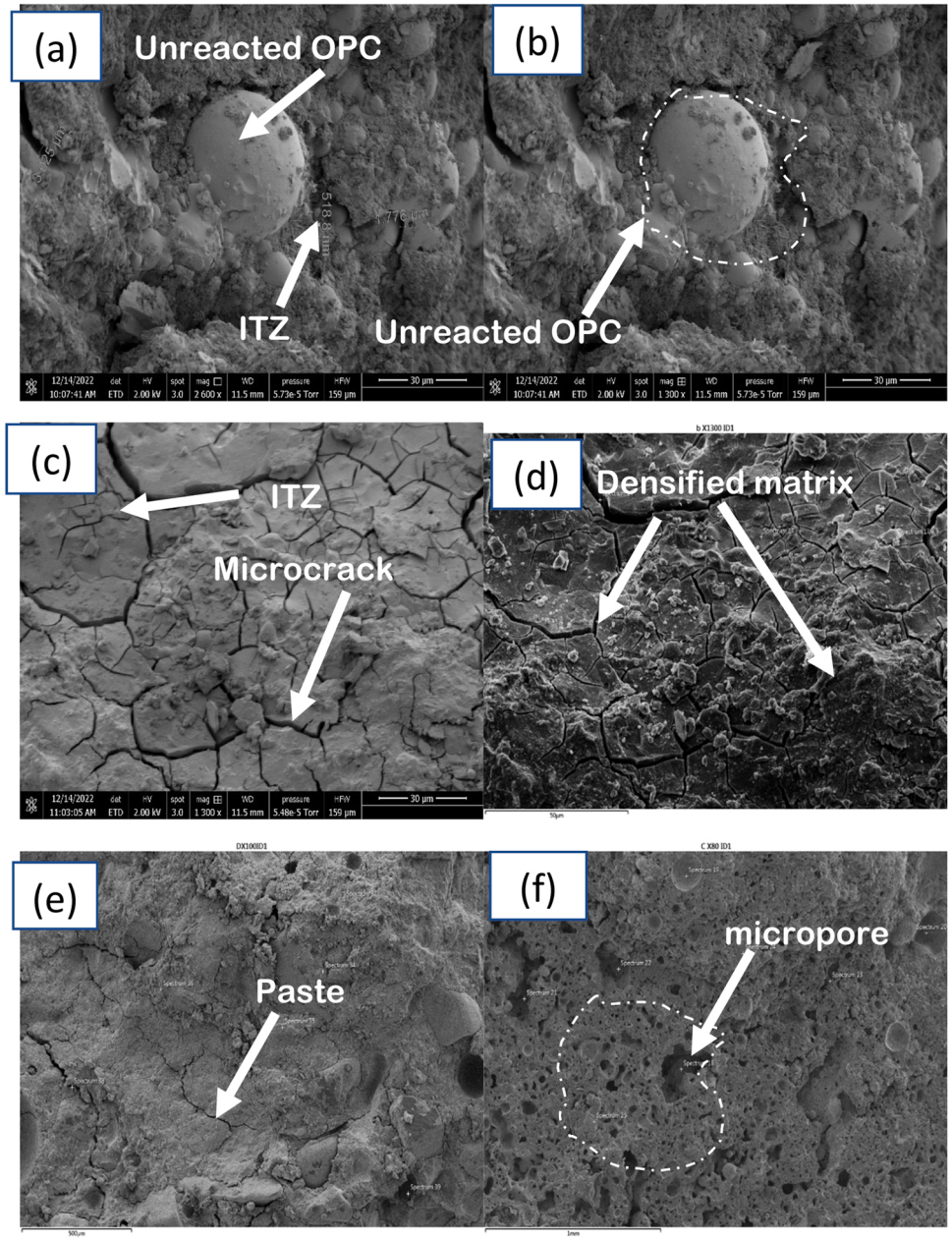

Fig. 19. SEM Micrograph of (a-b) LC30, (c-d) LC30/60, (e) LC20, (f) LC20/60, LC20/60, after 7 days of ambient curing.

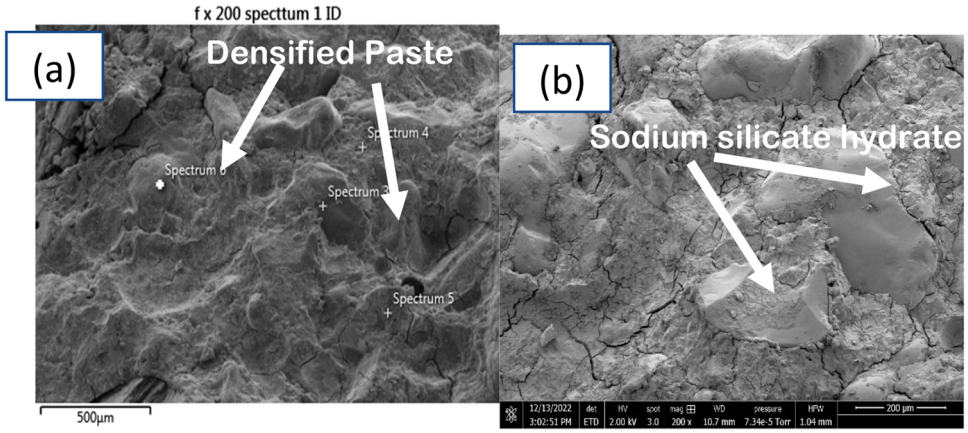

(a) LC20/60, (b) LC20/80 after 7 days of ambient curing

Fig. 20. SEM Micrograph.

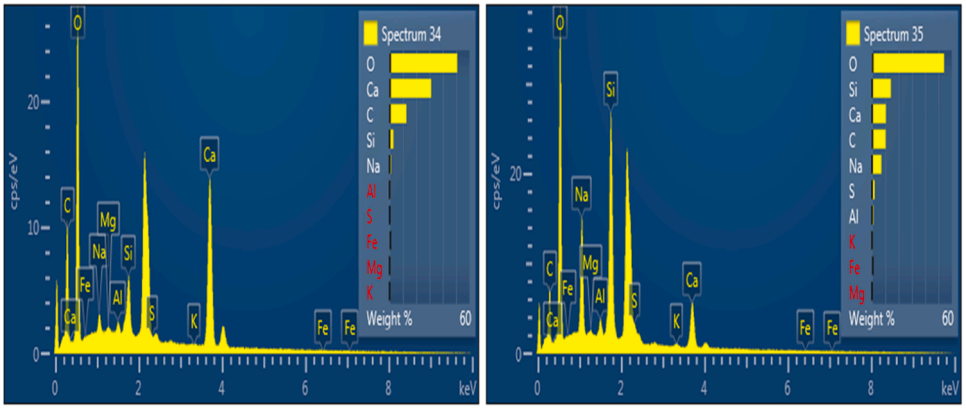

a: Spectrum 34 b: Spectrum 35

Fig. 21. (a-b): Spectral analysis for LC20/60.

Table 14
Spectral analysis for LC20/60.

Result type	Oxide composition (%) LC20/60									
Statistic	C	O	Na	Mg	Al	Si	S	K	Ca	Fe
Max	14.29	45.51	8.2	1.37	2.35	17.15	2.41	2.87	60.54	8.1
Min	8.29	18.94	1.05	0.22	0.42	3.2	0.43	0.16	12.52	0.37
Average	11.29	38.85	4.78	0.56	1.39	10.03	1.54	1.21	32.58	3.53
Standard Deviation	3.00	10.02	2.91	0.45	0.96	5.88	0.73	1	16.5	3.71

Table 15
Spectral analysis for LC20/70.

Result type	Oxide composition (%) LC20/70									
Statistic	C	O	Na	Mg	Al	Si	S	K	Ca	Fe
Max	13.53	51.64	6.57	5.38	4.88	21.35	2.18	1.34	40.61	0.7
Min	2.73	22.81	1.02	0.61	2.25	11.59	0.76	0.25	10.92	0.07
Average	10.07	45.69	4.96	1.93	3.07	14.07	1.35	0.69	17.72	0.44
Standard Deviation	3.62	9.39	1.73	1.84	1.04	3.18	0.43	0.3	9.77	0.19

of nano silica. This is obvious knowing that LC30 is 100% OPC, as there is also evidence to suggest that the exposure of sodium silicate to OPC resulted to the concrete deterioration. This is due to the formation of gypsum and ettringite because of its reaction with calcium hydroxide [87].

Results from the SEM analysis shows that as GGBS increases in the specimen, there is reduction in the composition of calcium and improvement in the mechanical performance, due to increase in the amount of silica. The increase in silica places a demand for more added free water and enhances effective hydration and good mechanical

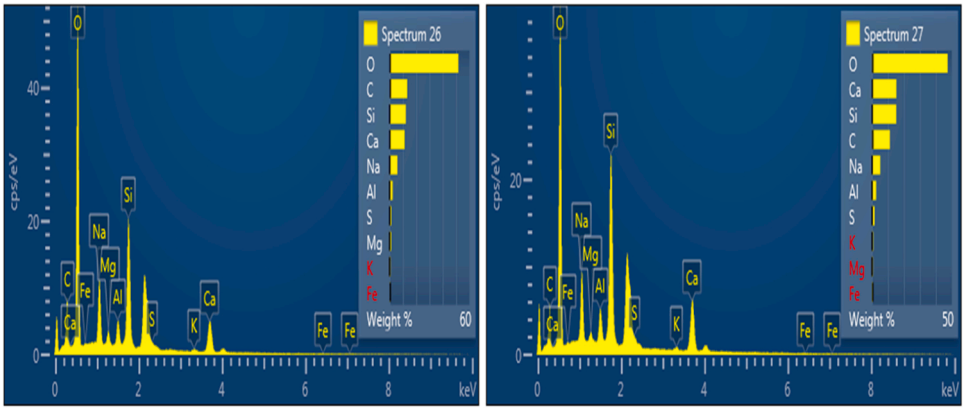

a: Spectrum 26 b: Spectrum 27

Fig22. (a-e): Spectral analysis for LC20/70.

Table 16
Spectral analysis for LC20/80.

Result type	Oxide composition (%) LC20/80									
Statistic	C	O	Na	Mg	Al	Si	S	K	Ca	Fe
Max	10.63	48.34	6.44	1.16	2.28	45.84	0.8	0.73	21.98	0.51
Min	5.8	39.71	0.13	0.03	0.19	19.18	0.3	0	0.44	0
Average	8.25	44.26	3.21	0.41	1.23	31.57	0.54	0.4	10.03	0.17
Standard Deviation	2.05	3.61	2.57	0.47	1.48	12.17	0.21	0.34	9.14	0.24

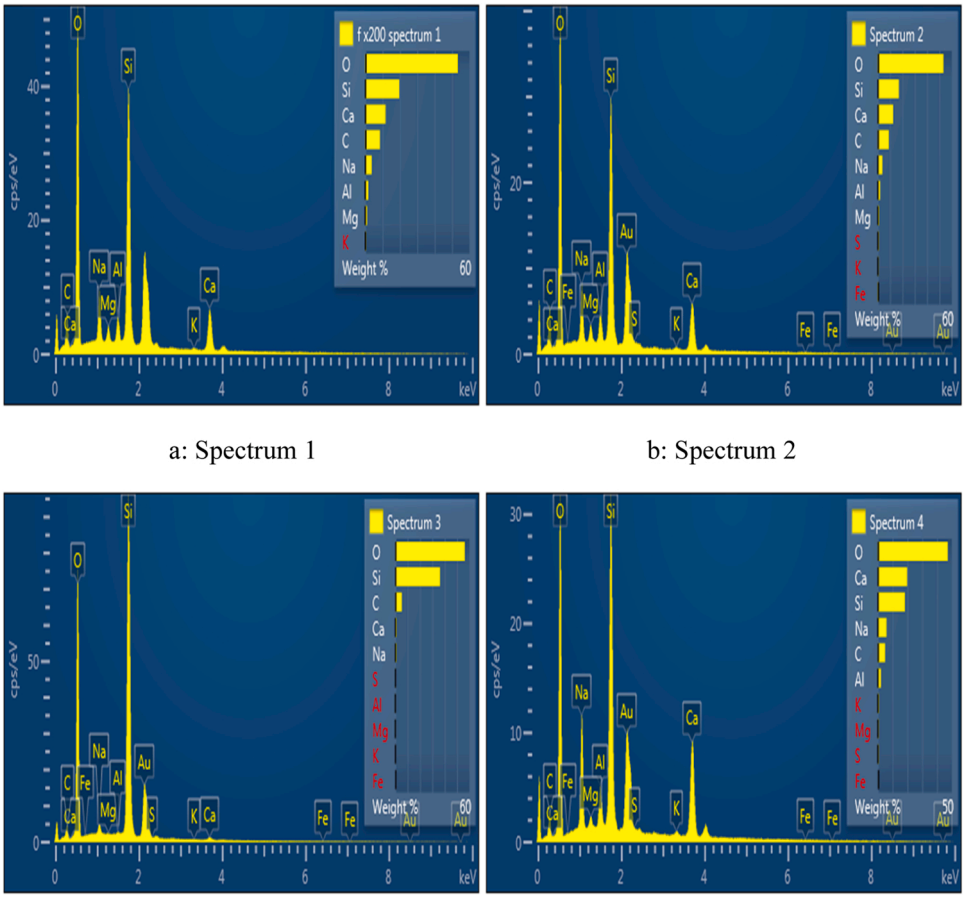

a: Spectrum 1 b: Spectrum 2

c: Spectrum 3 d: Spectrum 4

Fig. 23. (a-d): Spectral analysis for LC20/80.

Table 17
Spectral analysis for LC30/60.

Result type	Oxide composition (%) LC30/60								
Statistic	C	Na	Mg	Al	Si	S	K	Ca	Fe
Max	42.92	15.46	2.63	5.09	34.15	6.59	1.69	44.47	3.04
Min	8.69	6.42	0.67	3.95	20.21	1.95	0.43	13.06	1.11
Average	28.92	11.57	1.46	4.55	26.86	4.27	0.92	20.62	1.78
Standard Deviation	12.63	4.07	0.76	0.37	4.53	3.28	0.52	11.96	0.76

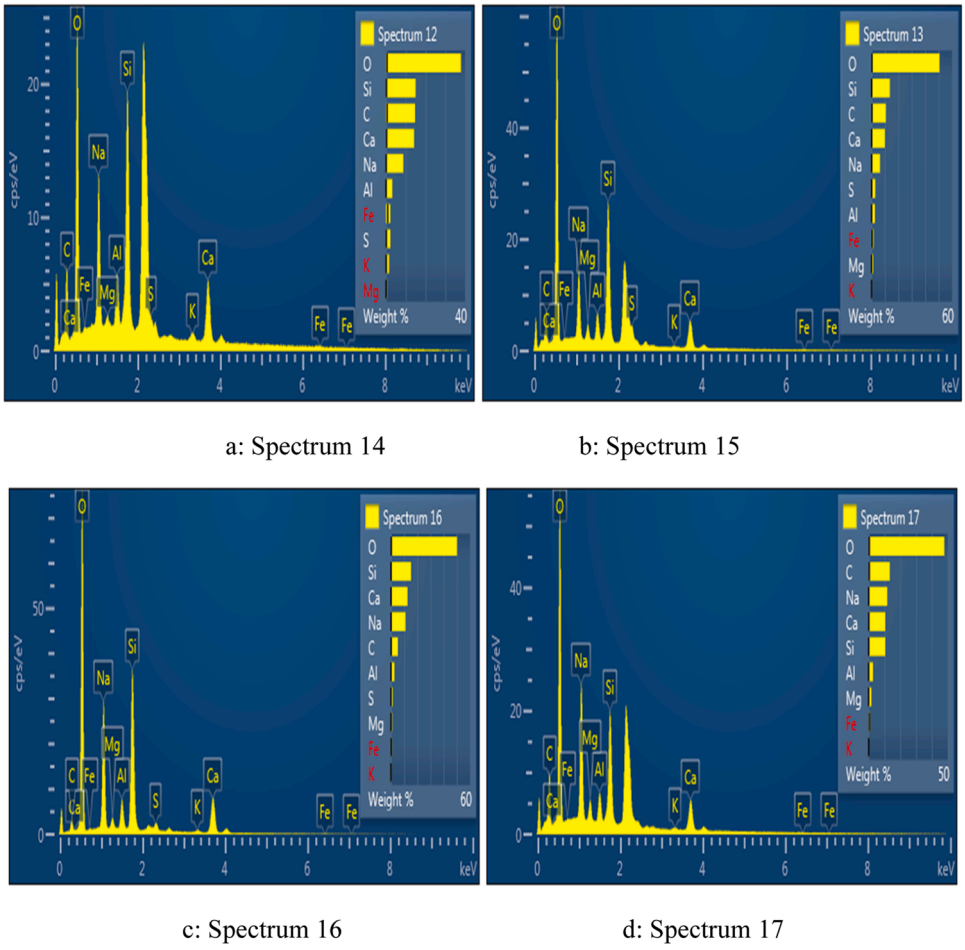

a: Spectrum 14 b: Spectrum 15

c: Spectrum 16 d: Spectrum 17

Fig. 24. (a-d): Spectral analysis for LC30/60.

a. Normal concrete grade 30 *b. Normal concrete grade 40*

Fig. 25. (a-b): Failure mode of sample.

performance.

3.8. Failure mode

Concrete failure has been noted for failure through vertical splitting in uniaxial compression with crack pattern parallel to the axis of load application. The build-up of large compressive stress characterises the formation of tensile stresses leading to failure of the concrete bond and eventual collapse. Tension and cracking are two fractures for failures used to describe compression test showing explosive cracks. The failure patterns are influenced by the bond between the paste and aggregate. The failures shown in Figs. 25 and 26 is typical of normal cracks, devoid of structural concerns.

Concrete composition influences the failure mode and its propagating from the weakest link. The weakest link for lightweight concrete is the aggregate as demonstrated by [88].

3.9. Creep Response

Evaluation of creep behaviour for lightweight concrete was carried out for 63days and compared with normal weight concrete for concrete grade 30 after 28-day curing. Creep is time dependent deformation of concrete under constant loading. Excessive creep effect in a structure causes failure of structural members. The complexity of the phenomenon of creep is occasioned by the several factors such as testing conditions, materials properties, curing conditions [89].

The phenomenon of creep is so important on a concrete structure which is obvious as the elastic deformation is small, when compared to increase of deformations from creep. The Creep coefficient $\psi(t, t_0)$ is calculated based on time functions of total strain, shrinkage strain and elastic strain. This is expressed in Eq. 9 as:

$$\psi(t, t_0) = \beta cp(t, to)/\Upsilon e(to) \tag{9}$$

Where $\beta cp(t, to) = \beta c(t) - \Upsilon s(t) - \Upsilon e(to)$,

$\beta c(t, to)$ is creep strain as a function of t and to,

$\beta c(t)$ is the total strain of the concrete at age t,

$\Upsilon e(to)$ is the initial elastic modulus at age to,

$\Upsilon s(t)$ is the shrinkage strain at age t

The Deformation of concrete due to creep is likely to reduce the strength of concrete as the initial elastic modulus, the initial elastic modulus, E_c during the process of creep attains a final elastic modulus, E_f value given in Eq. 10 as:

$$E_f = \frac{E_c}{1+\theta} \tag{10}$$

where θ is the creep coefficient, which is express in Eq. 11 as:

$$\theta = \frac{Ultimate \quad strain \quad at \quad instant \quad of \quad age}{Initial \text{elastic} strain} \tag{11}$$

Creep coefficient is the ratio of the long-term strain to the short-term strain when a material undergoes stress over a long period.

Creep test was carried out using ACONS Pro Motorised Automatic Consolidation System have a 15 kN (2176 psi) Load Cell. Due to constraint of equipment for the creep test, the applied load was limited to 15 kN. Constant rate of strain of the concrete was measured using digital input channel under control temperature of 29 ± 1^0 C and 65 ±4% relative humidity. A sustained load of 8% of compressive strength of NWC30, LC30, and LC30/60 was applied on each specimen. Development of creep stress is induced by the instantaneous elastic strain when loaded in compression. The creep strain developed is expressed as a ratio of elastic strain and is used to describe the long-term deformation of concrete. When it is divided by instantaneous elastic strain, it is known as creep coefficient. Compressive test on similar mix and concrete grade for the specimen prior to the creep test were carried out. A

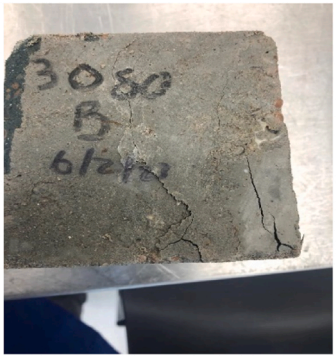

a. LC30/60

b. Normal concrete grade 20

c. Normal concrete grade 50

d. Flexural test failure

Fig. 26. (a-d): Failure mode of concrete sample after crushing.

load of 15 kN was applied on the specimen during the creep test and the induced stress, δ_m is calculated using Eq. 12 as:

$$\delta_m = \frac{1000Pn}{lx\omega} = \frac{1000x15}{75x75} = 2.66\ \text{N}\Big/\text{mm}^2 \quad = 2.7(\text{Mpa}) \tag{12}$$

Compressive strength of NW30, LC30 and LC30/60 specimen are 35.96, 33.11 and 43.5 MPa.

The percent load applied falls within the range 0–50% as required [90].

The performance of lightweight concrete in terms of creep has been described by previous studies to be relatively poor, however the addition of silica fume has shown to enhances significant improvement [91–93]. Lightweight concrete is known for high creep coefficient compared to normal weight concrete owing to its low stiffness value [94]. The creep testing is caried out to comply with ASTM C512 [90]. Three rectangular creep and shrinkage specimen were prepared. The three specimens were cured for 28days, placed in the test frame, and loaded at 8% of their compressive strength. Deformations were monitored on digital screen as shown in Fig. 28. The experimental set up for the creep test carried out are as shown in Fig. 27. Three rectangular prisms of size 75 ×75×280 mm were prepared.

3.9.1. Experimental results

Creep properties were measured by analysing the development of creep strain with focused on compressive stress. The component of total strain is considered to include instantaneous elastic strain, shrinkage strain and creep strain as expressed in Eq. 13 to evaluate the concrete behaviour.

$$\varepsilon_t = \varepsilon_{el} + \varepsilon_{cr} + \varepsilon_{st} + \varepsilon_{th} \tag{13}$$

where, ε_t is total strain; ε_{el} is elastic strain; ε_{cr} is creep strain; ε_{sh} is shrinkage strain; ε_{th} is thermal strain. The thermal strain is neglected in this study, since the samples were kept in constant temperature of 20 ± 1^0 C. Creep coefficient of the concrete specimen obtained are presented in Fig. 28 and other creep properties in Tables 18 – 20. The cracking stress of lightweight aggregates when prewetted decreases as the number of aggregates increases and resulted to increase in cracking stress to tensile strength ratio. Studies shows that this increase is due to reduction in the elastic modulus of the lightweight aggregate compared to the normal weight aggregate. This potential effect reduces internal microcracking and lowers the risk of cracking in the concrete [95]. This agrees with the observation in this study as noted in Table 19, with the reduction in elastic modulus of LC30/60 and LC30 compared to increase in that of NWC30 between 7 and 63 days of loading.

In comparing creep performance of lightweight concrete with that of normal weight concrete, similar studies shows that lightweight concrete exhibited 60% creep strain, greater than the normal weight concrete within 28 days of load [96]. From this study, it was observed that creep strain between 7 and 63 days, increased by 0.55% for LC30/60, increased by 2.81% for LC30 but reduced by 28.12% for NWC30. This increases as noted for LC30/60 when compared to LC30, is suggested to be influenced by enhanced hydration and a densified microstructure of the cementitious paste, which is noted for enhanced resistance to creep. With the creep performance exhibited, there is need to suggest that the concrete microstructure is densified with the formation of smaller aggregates, within the aggregate due to polymerization.

The presence of "micro-aggregates" in geopolymer concrete due to the block-polymerization concept is highlighted as a factor that increases the creep resistance of the material.[97]. Creep strain obtained for PFA geopolymer range from 500 to 2500 micro strains [98], which compares favourably to 616.28 for LC30/60 and 628.61 micro strains for LC30 obtained in this study as shown in Fig. 28. It is also observed that Creep coefficient of LC30/60 is lower compared to LC30. The improvement in creep strains for geopolymer concrete which is noted on LC30/60 compared to LC30 is suggested to be due to geo-polymerisation. Creep resisting functions of the geopolymer concrete (LC30/60) is due to the formation of smaller aggregates within the aggregate due to polymerization. When compared with their compressive strength, it is noted that creep reduces with increasing compressive strength of the geopolymer concrete. Low creep strain as associated with higher percentage cement replacement with GGBS have been reported [89] and is suggested to be due to more free water requirement which resulted to slow strength development. For the mix constituents of LC30/60, there was no added free water, hence the reduction in creep strain. Also due to high-water demand of concrete, stress is easily redistributed within the material when place under stress and can contribute to increased drying shrinkage and cracking in concrete as excess water evaporates during curing.

3.9.2. Modulus of elasticity

Creep performance exhibited by the concrete is presented in Table 20 for the test specimen. The creep strains and instantaneous elastic strain increase at 0.55% between 7 and 28 days of loading for the LC30/60 specimen compared to 2.81% for LC30, however reduction in creep strain for NWC 30 specimen is 28.17%.The improvement in creep strain for the lightweight GGBS LYTAG blended geopolymer compared to LC30 is justified with added alkaline solution and resulted to slight reduction

a. Set up for creep test

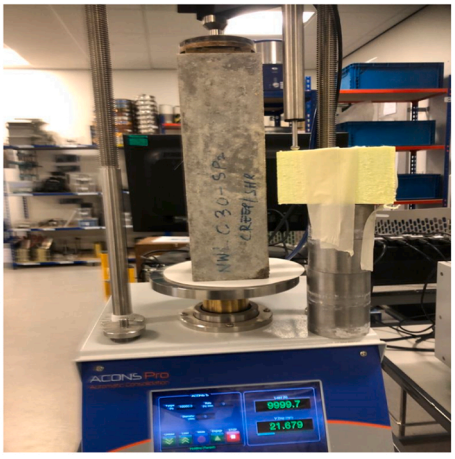

b. sample under loading.

Fig. 27. (a-b): Concrete creep test.

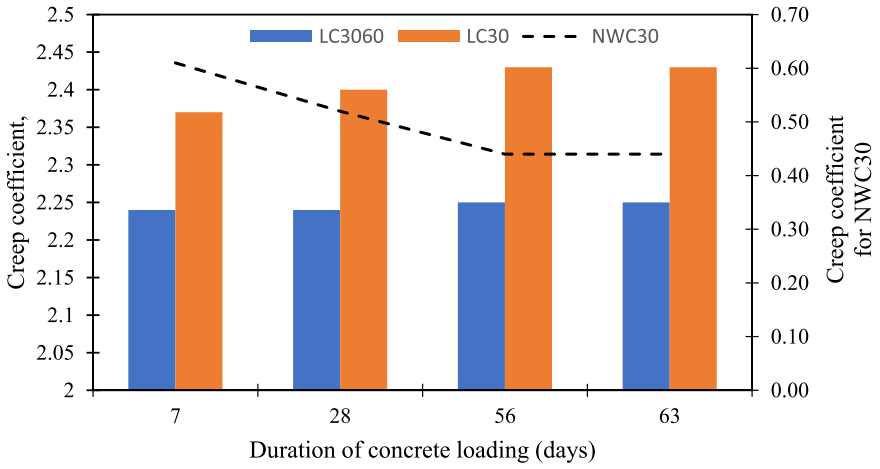

Fig. 28. creep strain of concrete specimen after 28 days of curing and loaded for 63 days.

Table 18
63-day creep coefficient for Lytag-GGBS Geopolymer and Normal weight concrete.

Specimen	Concrete density (kg/m^3)	Instantaneous Elastic Strain (micro stain)	Creep Strain at 63 days (micro strain)	Predicted Creep Strain. Eq. 14 (micro strain)	Modulus of Elasticity at 63 days (kN/mm^2)	Creep coefficient $\frac{Col.4}{Col.3}$
(1)	(2)	(3)	(4)	(5)	(6)	(7)
LC30/60	1808	273.82	616.28	625	84.24	2.25
LC30	1863	258.10	628.61	629	75.13	2.43
NWC30	2357	208.91	92.00	91	144.93	0.44

Table 19
Modulus of Elasticity (kN/mm^2).

Specimen	Duration of concrete loading (days)			
	7	28	56	63
LC30/60	84.56	84.39	84.26	84.23
LC30	76.61	75.85	75.27	75.13
NWC30	129.4	137.09	144.45	144.93

Table 20
Creep coefficient of the concrete sample after 28 days curing and loaded for 63 days.

Specimen	Duration of concrete loading(days)			
	7	28	56	63
LC30/60	2.24	2.24	2.25	2.25
LC30	2.37	2.4	2.43	2.43
NWC30	0.61	0.52	0.44	0.44

in the modulus of elasticity (MoE) as shown in Table 19 and reduced creep coefficient in Table 20. The result also shows that MoE for LC30/60 reduces by 0.39% between 7 and 63 days of loading while that of LC30 reduced by 1.93% and NWC30 increased by 12%. The modulus of elasticity of the geopolymer is shown to be 58% to the value of the normal weight concrete under creep load. This can attributed to the density of the concrete.

3.9.3. Creep coefficient

The creep coefficient is a crucial parameter that characterizes the time-dependent deformation of concrete under sustained loading. It has been reported that the lower creep and creep coefficient values of geopolymer concrete contribute to its improved performance characteristics compared to traditional concrete materials [99]. Similar studies conducted for PFA blended geopolymer shows 45% lower creep coefficient compared to that of normal weight concrete [100]. Evaluation of the behaviour and properties of Lytag sand concrete from previous study suggest that value of creep coefficient for a target mix of 30 MPa of 3.58 after 100 days of loading compared with 2.43 obtained in this study [22]. It can be observed that about 50% of the ultimate creep strain occurred within 2 days after loading and more than 90% were attained between 10 and 63 days after loading. A significant reduction in creep coefficient at 7.41% is noted between LC30/60 and LC30. The impact of alkaline solution is noted in the result for LC30/60 and LC30 with an improved creep performance. Alkaline solution appears to impact the creep behaviour through cement hydration process which is shown in Fig. 28 with a lower creep coefficient. Creep response of the concrete specimen as shown in Fig. 29 provide the pattern of response to stress under load. It is observed that for the LC30/60 sample, there is small increase in the creep strain as the duration of loading increases when compared with LC30 which emphasizes concrete structural resilience.

Creep prediction using simple hyperbolic equation have been presented in lambert [22] to describe the behaviour of concrete under creep or shrinkage. This is expressed as:

$$c = \frac{t}{a + bt} \tag{14}$$

Where C = predicted creep strain (micro strain), t = time after loading (days), a and b are constants. To determine a and b, rearrangement of equation was carried out, knowing that as t approaches infinity, the limiting value of C = 1/b. This implies that a and b can be obtained using equation15 as:

$$\frac{t}{Ce} = bt + a \tag{15}$$

Where Ce is the experimental creep strain. From the plot of $\frac{t}{Ce}$ against t, the slope, b was evaluated as 0.0016 and the intercept a as 0. With a and b obtained, the predicted creep strain was determined and presented in

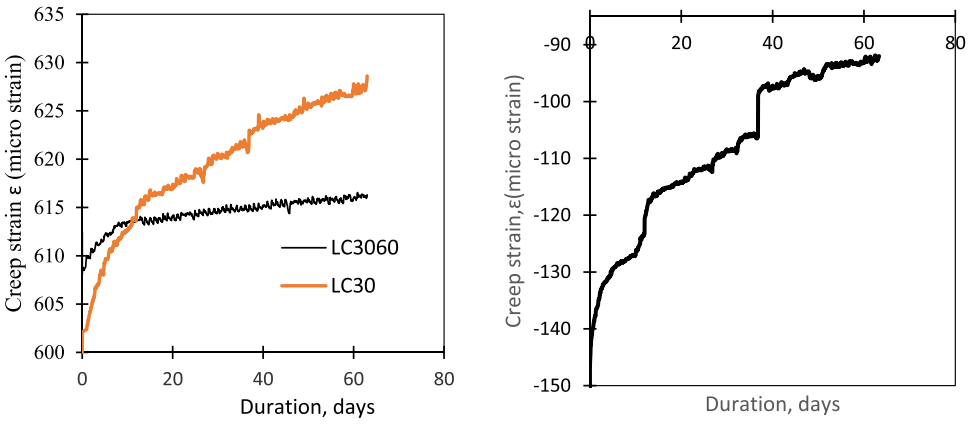

a. Lightweight concrete (LC30 & LC3060) *b. Normal weight concrete (NWC30)*

Fig. 29. (a-b): Creep strain of concrete specimen cured for 28 days and loaded for 63 days.

Table 18 which indicates good similarity with the measured creep strain from this study.

3.10. Conclusion and recommendation for future direction

The development of a green geo-polymer-based concrete using Lytag aggregate, and Ground Granular Blast-furnace Slag (GGBS) activated with an alkaline solution of 15 M sodium hydroxide as a precursor, was studied. It has been reported from previous studies that issues of workability and poor strength development is associated with poor performance of GGBS in concrete. However, the outcome of this present study showed that the inclusion of silica fume and superplasticizer mitigate the issues of poor strength development and enhance good structural performance of GGBS based geo-polymer concrete in terms creep response and stress strain behaviour. The result present potentials for the development of advanced material models such as nonlinear finite element model since they depend on accurate representation of stress strain behaviour to simulate the response of concrete structures. This which would impact on various aspect of design equation for the design of light weight concrete in terms of strength prediction, ductility assessment, reinforcement design and development of advanced materials models.

From the experimental program carried out, the following were concluded.

- Due to high water absorption of Lytag, when it is used as an aggregate in geopolymer concrete, optimization of added free water is suggested, but not exceeding the A/B ratio for effective hydration. Optimal performance of the concrete occurs at 80% GGBS replacement for concrete grade 20, 60% GGBS for concrete grade 30 and 70% GGBS for concrete grade 40.
- GGBS Lytag silica fume blended geopolymer concrete gains 84% of its 28 days compressive strength within 7 days of age while that of the flexural strength gains 24% of its 28 days strength with 7 days of age.
- The use of Lytag silica fume lightweight concrete results to 46.1–61.92% reduction in embodied carbon while the geopolymer green concrete reduces embodied carbon by 69.19–73% for 60% GGBS, 73–75% for 70% GGBS and 76.87–77% for 80% GGBS.
- Increases in GGBS composition for geopolymer concrete from 60% to 80% results to 64% increase in silica and 63% reduction in calcium composition in the concrete specimen which lead to increase in compressive strength by 14.40%.
- The value of Measured fresh density of the GGBS Lytag geopolymer lightweight concrete falls within the limit as recommended by ASTM C567 to enhance the relationship between oven dried density and equilibrium density of light weight concrete.
- GGBS blended geopolymer concrete exhibited reduction in modulus of elasticity with increase in age of loading at 0.39% while that of the non-geopolymer concrete reduces at 1.93% between 7 and 63days of loading and normal weight concrete increase by 12%.
- Creep strain of the geopolymer concrete after 63days of loading reduces by 0.1% compared to increase of 2.56% for non-geopolymer lytag based concrete and 1.72% for normal weight concrete. The creep performance is suggested to be due to the densified microstructure of geopolymer concrete due to alkaline polymerization and reduction in concrete water demand.
- Due to the high-water demand of lytag aggregate, the use of lytag aggregate requires a 24hrs pre-soaked in water before use for concrete preparation. SEM results on the specimen indicates a high composition of silica in the concrete making lytag to present pozzolanic activities. Studies should be extended to investigate microstructural characteristics of the concrete at the different duration of pre-soaking. Also, the bonding effect with reinforcement of lightweight geopolymer concrete should be carried out as there is minor decline in flexural strength compared to the conventional normal weight concrete.

CRediT authorship contribution statement

samuel abbey: Writing – review & editing, Visualization. **Promise Nukah:** Writing – original draft, Methodology, Formal analysis, Conceptualization. **Jonathan Oti:** Investigation, Data curation. **colin Booth:** Supervision, Project administration.

Declaration of Competing Interest

The authors declare that they have no known competing financial interests or personal relationships that could have appeared to influence the work reported in this paper.

Data Availability

Data will be made available on request.

Acknowledgement

The authors would like to specially thank the University of the West of England, Bristol for funding this PhD Research project under the grant number 7911422.

Appendix A. Supporting information

Supplementary data associated with this article can be found in the online version at doi:10.1016/j.conbuildmat.2024.136295.

References

[1] S.A. Zareei, F. Ameri, N. Bahrami, P. Shoaei, H.R. Moosaei, N. Salemi, Performance of sustainable high strength concrete with basic oxygen steel-making (BOS) slag and nano-silica, J. Build. Eng. 25 (2019) 100791, https://doi.org/10.1016/j.jobe.2019.100791.

[2] Y.H.M. Amran, R. Alyousef, H. Alabduljabbar, M. El-Zeadani, Clean production and properties of geopolymer concrete; A review, J. Clean. Prod. 251 (2020) 119679, https://doi.org/10.1016/j.jclepro.2019.119679.

[3] N. Mahasenan, S. Smith, K. Humphreys, The cement industry and global climate changecurrent and potential future cement industry CO2 emissions, Greenh. Gas. Control Technol. - 6th Int. Conf. (2003) 995–1000, https://doi.org/10.1016/b978-008044276-1/50157-4.

[4] S. Mengxiao, W. Qiang, Z. Zhikai, Comparison of the properties between high-volume fly ash concrete and high-volume steel slag concrete under temperature matching curing condition, Constr. Build. Mater. 98 (2015) 649–655, https://doi.org/10.1016/j.conbuildmat.2015.08.134.

[5] A. Attari, C. McNally, M.G. Richardson, A combined SEM–Calorimetric approach for assessing hydration and porosity development in GGBS concrete, Cem. Concr. Compos. 68 (2016) 46–56, https://doi.org/10.1016/j.cemconcomp.2016.02.001.

[6] M. Amran, G. Murali, N.H.A. Khalid, R. Fediuk, T. Ozbakkaloglu, Y.H. Lee, S. Haruna, Y.Y. Lee, Slag uses in making an ecofriendly and sustainable concrete: A review, Constr. Build. Mater. 272 (2021) 121942, https://doi.org/10.1016/j.conbuildmat.2020.121942.

[7] S. Samad, A. Shah, Role of binary cement including supplementary cementitious material (scm), in production of environmentally sustainable concrete: a critical review, Int. J. Sustain. Built Environ. 6 (2) (2017) 663–674, https://doi.org/10.1016/j.ijsbe.2017.07.003.

[8] W. Wang, T. Noguchi, Alkali-silica reaction (ASR) in the alkali-activated cement (AAC) system: A state-of-the-art review, Constr. Build. Mater. 252 (2020) 119105, https://doi.org/10.1016/j.conbuildmat.2020.119105.

[9] G. Hammond, C. Jones, F. Lowrie, P. Tse, Building Services Research And Information Association and University Of Bath, Embodied carbon: the Inventory of Carbon and Energy (ICE), Bsria, Bracknell, 2011.

[10] R. Siddique, R. Bennacer, Use of iron and steel industry by-product (GGBS) in cement paste and mortar, Resour., Conserv. Recycl. 69 (2012) 29–34, https://doi.org/10.1016/j.resconrec.2012.09.002.

[11] J. Zhao, D. Wang, P. Yan, Design and experimental study of a ternary blended cement containing high volume steel slag and blast-furnace slag based on Fuller distribution model, Constr. Build. Mater. 140 (2017) 248–256, https://doi.org/10.1016/j.conbuildmat.2017.02.119.

[12] J.J. Gaitero, I. Campillo, A. Guerrero, Reduction of the calcium leaching rate of cement paste by addition of silica nanoparticles, Cem. Concr. Res. 38 (8–9) (2008) 1112–1118.

[13] Kanavaris, F., Gibbons, O., Walport, E., Shearer, E., Abbas, A., Orr, J. and Marsh, B. (2021) Reducing embodied carbon dioxide of structural concrete with lightweight aggregate. Proceedings of the Institution of Civil Engineers - Engineering Sustainability. [online]. pp.1–9.

[14] J. Fořt, M. Mildner, M. Keppert, M. Abed, R. Černý, Potential of industrial waste as alternative alkaline activator for development of eco-efficient mortars, Case Stud. Constr. Mater. (2022) e01716.

[15] K. Lal Jain, L. Singh Rajawat, G. Sancheti, Mechanical Properties of Ground Granulated Blast Furnace Slag Made Concrete, IOP Conf. Ser.: Earth Environ. Sci. 796 (1) (2021) 012063.

[16] D.J.M. Flower, J.G. Sanjayan, Greenhouse gas emissions due to concrete manufacture, Int. J. Life Cycle Assess. 12 (5) (2007) 282–288.

[17] J. Ahmad, K.J. Kontoleon, A. Majdi, M.T. Naqash, A.F. Deifalla, N. Ben Kahla, H. F. Isleem, S.M.A. Qaidi, A Comprehensive Review on the Ground Granulated Blast Furnace Slag (GGBS) in Concrete Production, Sustainability 14 (14) (2022) 8783.

[18] P.D. Nukah, S.J. Abbey, C.A. Booth, G. Nounu, Optimisation of Embodied Carbon and Compressive Strength in Low Carbon Concrete, Materials 15 (23) (2022) 8673.

[19] K.-C. Hsu, J.-J. Chiu, S.-D. Chen, Y.-C. Tseng, Effect of addition time of a superplasticizer on cement adsorption and on concrete workability, Cem. Concr. Compos. 21 (5–6) (1999) 425–430.

[20] Clarke, D.J.L. (2002) Structural Lightweight Aggregate Concrete CRC Press.

[21] Concrete Society Technical Report (1978) Structural lightweight aggregate concrete for marine and offshore applications Report of a Concrete Society working party.

[22] Lambert, G. (1982) Properties and behaviour of Structural Light Weight (Lytag-Sand) Concrete University of Sheffield, 1–304.

[23] K.H. Mo, T.-C. Ling, T.H. Tan, G.W. Leong, C.W. Yuen, S.N. Shah, Alkali-silica reactivity of lightweight aggregate: A brief overview, Constr. Build. Mater. 270 (2021) 121444.

[24] G. Samson, A. Phelipot-Mardelé, C. Lanos, A review of thermomechanical properties of lightweight concrete, Mag. Concr. Res. 69 (4) (2017) 201–216.

[25] P.D. Nukah, S.J. Abbey, C.A. Booth, G. Nounu, Development of a Lytag-silica fume based lightweight concrete and corresponding design equation for pure bending, Case Stud. Constr. Mater. (2023) e01970.

[26] H.K. Kim, J.H. Jeon, H.K. Lee, Workability, and mechanical, acoustic and thermal properties of lightweight aggregate concrete with a high volume of entrained air, Constr. Build. Mater. 29 (2012) 193–200.

[27] C.-W. Tang, H.-J. Chen, S.-Y. Wang, J. Spaulding, Production of synthetic lightweight aggregate using reservoir sediments for concrete and masonry, Cem. Concr. Compos. 33 (2) (2011) 292–300.

[28] R. Wasserman, A. Bentur, Effect of lightweight fly ash aggregate microstructure on the strength of concretes, Cem. Concr. Res. 27 (4) (1997) 525–537.

[29] R.N. Swamy, G.H. Lambert, The microstructure of Lytag aggregate, Int. J. Cem. Compos. Lightweight Concr. 3 (4) (1981) 273–282.

[30] S. Ahmad, Y.S. Sallam, I.A.R. Al-Hashmi, Optimising dosage of Lytag used as coarse aggregate in lightweight aggregate concretes, J. SOUTH Afr. Inst. Civ. Eng. 55 (1) (2013) 80–84.

[31] A. Palomo, M.W. Grutzeck, M.T. Blanco, Alkali-activated fly ashes, Cem. Concr. Res. 29 (8) (1999) 1323–1329.

[32] A.A. Ensafi, N. Kazemifard, Z. Saberi Dehkordi, Parameters that affect molecular imprinting polymers, Mol. Impr. Polym. Compos. (2021) 21–48, https://doi.org/10.1016/b978-0-12-819952-7.00010-x.

[33] S. Parathi, P. Nagarajan, S.A. Pallikkara, Ecofriendly geopolymer concrete: a comprehensive review, Clean. Technol. Environ. Policy 23 (6) (2021) 1701–1713, https://doi.org/10.1007/s10098-021-02085-0.

[34] A.R. Brough, A. Katz, G.-K. Sun, L.J. Struble, R.J. Kirkpatrick, J.F. Young, Adiabatically cured, alkali-activated cement-based wasteforms containing high levels of fly ash, Cem. Concr. Res. 31 (10) (2001) 1437–1447.

[35] U. Rattanasak, P. Chindaprasirt, Influence of NaOH solution on the synthesis of fly ash geopolymer, Miner. Eng. 22 (12) (2009) 1073–1078.

[36] X. Guo, H. Shi, W.A. Dick, Compressive strength and microstructural characteristics of class C fly ash geopolymer, Cem. Concr. Compos. 32 (2) (2010) 142–147.

[37] K. Kalinowska-Wichrowska, E. Pawluczuk, M. Bołtryk, A. Nietupski, Geopolymer Concrete with Lightweight Artificial Aggregates, Materials 15 (9) (2022) 3012, https://doi.org/10.3390/ma15093012.

[38] B. Singh, G. Ishwarya, M. Gupta, S.K. Bhattacharyya, Geopolymer concrete: A review of some recent developments, Constr. Build. Mater. 85 (2015) 78–90, https://doi.org/10.1016/j.conbuildmat.2015.03.036.

[39] P. Duxson, A. Fernández-Jiménez, J.L. Provis, G.C. Lukey, A. Palomo, J.S.J. van Deventer, Geopolymer technology: the current state of the art, J. Mater. Sci. 42 (9) (2006) 2917–2933, https://doi.org/10.1007/s10853-006-0637-z.

[40] British Standards Institution (2011) BS EN 197-1: 2011. Cement. Composition, Specifications and Conformity Criteria for Common Cements. British Standards Institution, London.

[41] BS EN 15167-1:2006. Ground granulated blast furnace slag for use in concrete, mortar and grout Definitions, specifications and conformity criteria.

[42] BS EN 933-1:2012. Tests for geometrical properties of aggregates Determination of particle size distribution. Sieving method.

[43] S. Sarker, M.A. Hossain, O.C. Debnath, N. Tabassum, M.S. Islam, Strength behaviour of Slag (GGBS) based Geopolymer Concrete in Chlorine Environment (December), *Proc. 3rd Int. Conf. Adv. Civ. Eng.* (2016) *21–23*.

[44] M.N.S. Hadi, N.A. Farhan, M.N. Sheikh, Design of geopolymer concrete with GGBFS at ambient curing condition using Taguchi method, Constr. Build. Mater. 140 (2017) 424–431, https://doi.org/10.1016/j.conbuildmat.2017.02.131.

[45] H.M. Tanu, Sujatha Unnikrishnan, Mechanical Strength and Microstructure of GGBS-SCBA based Geopolymer Concrete, J. Mater. Res. Technol. 24 (2023) 7816–7831, https://doi.org/10.1016/j.jmrt.2023.05.051.

[46] A. Chithambar Ganesh, P. Siva Kumar, S. Kapilan, A. Kumar, Shaik Nazeer Basha, Veeramsetti Tejaeswar, Effect of alkaline activator solution over GGBS based concrete under ambient curing, Mater. Today.: Proc. (2023), https://doi.org/10.1016/j.matpr.2023.07.159.

[47] K.K. Singaram, M.A. Khan, V. Talakokula, Statistical analysis of fly ash and slag blended geopolymer concrete, Mater. Today.: Proc. 61 (2022) 466–476, https://doi.org/10.1016/j.matpr.2021.12.026.

[48] T. Harrison, British Standards Institution, Standards for Fresh Concrete: The Application of BS EN 206-1 and BS 8500, British Standards Institution, London, 2004.

[49] R.N. Swamy, G.H. Lambert, Mix design and properties of concrete made from PFA coarse aggregates and sand, Int. J. Cem. Compos. Lightweight Concr. 5 (4) (1983) 263–275, https://doi.org/10.1016/0262-5075(83)90068-4.

[50] BS EN 1992-1-1:2004. Eurocode 2: Design of concrete structures – Part 1-1: General rules and rules for buildings. *British Standards Institute*, U.K., pp. 29, 33, 187, 189.

[51] ASTM International - ASTM C567/C567M-14 (2014) Standard Test Method for Determining Density of Structural Lightweight Concrete ASTM international.

[52] BS EN 12390-3 (2009) Testing Hardened Concrete—Part 3: Compressive Strength of Test Specimens. Management Centre, Brussels.

[53] ASTM C293. "Standard Test Method for Flexural Strength of Concrete Using Simple Beam With Center-Point Loading." Annual book of ASTM standards

[54] British Standards Institution (Bsi (2019) BS EN 12390-5:2019. *Testing hardened concrete. Part 5 : Flexural strength of test specimens* Bsi.

[55] K.T. Nguyen, N. Ahn, T.A. Le, K. Lee, Theoretical and experimental study on mechanical properties and flexural strength of fly ash-geopolymer concrete, Constr. Build. Mater. 106 (2016) 65–77, https://doi.org/10.1016/j.conbuildmat.2015.12.033.

[56] BS EN 12350. Part 2. Testing fresh concrete: slump test. London: BSI; 2000.

[57] Y.-W. Zhou, Y.-F. Wu, General model for constitutive relationships of concrete and its composite structures, Compos. Struct. 94 (2) (2012) 580–592.

[58] L. Ahmed, Dynamic Measurements for Determining Poisson's Ratio of Young Concrete, Nord. Concr. Res. 58 (1) (2018) 95–106, https://doi.org/10.2478/ncr-2018-0006.

[59] L. Domagała, The Effect of Lightweight Aggregate Water Absorption on the Reduction of Water-cement Ratio in Fresh Concrete, Procedia Eng. 108 (2015) 206–213, https://doi.org/10.1016/j.proeng.2015.06.139.

[60] P.D. Nukah, S.J. Abbey, C.A. Booth, Ghassan Nounu, Mapping and synthesizing the viability of cement replacement materials via a systematic review and meta-analysis, 133290–133290, Constr. Build. Mater. 405 (2023), https://doi.org/10.1016/j.conbuildmat.2023.133290.

[61] Anbarasan, I. and Soundarapandian, N. (2019) Investigation of mechanical and micro structural properties of geopolymer concrete blended by dredged marine sand and manufactured sand under ambient curing conditions. *Structural Concrete* [online].

[62] KIRAN KUMAR POLOJU and Kota Sinivasu (2023) Influence of GGBS and Alkaline Ratio on Compression Strength of Geopolymer Concrete: Influence of GGBS and Alkaline Ratio on Compression Strength of Geopolymer Concrete. *SPAST Abstracts* [online]. 1 (01). Available from: ⟨https://spast.org/techrep/article/view/2900⟩ [Accessed 26 June 2023].

[63] Luo, Z., Li, W., Gan, Y., He, X., Castel, A. and Sheng, D. (2021) Nanoindentation on micromechanical properties and microstructure of geopolymer with nano-SiO2 and nano-TiO2. *Cement and Concrete Composites* [online]. 117, p. 103883. Available from: ⟨https://reader.elsevier.com/reader/sd/pii/S0958946520303875?token=F09D7E7D5A8CCCEE844E292388AC7A992B6249A64B8531A556F9EFE1E0C820B5CB3C019CBB4B69C302045144D94D3022&originRegion=eu-west-1&originCreation=20221201114402⟩ [Accessed 1 December 2022].

[64] Y. Ding, C.-J. Shi, N. Li, Fracture properties of slag/fly ash-based geopolymer concrete cured in ambient temperature, Constr. Build. Mater. 190 (2018) 787–795. Accessed 13 July 2020].

[65] Mazloom, M., Soltani, A., Karamloo, M., A. Hassanloo and Ranjbar, A. (2018) Effects of silica fume, superplasticizer dosage and type of superplasticizer on the properties of normal and self-compacting concrete. [online]. 7 (1), p. 45. [Accessed 19 June 2023].

[66] R. Ghostine, N. Bur, F. Feugeas, I. Hoteit, Curing Effect on Durability of Cement Mortar with GGBS: Experimental and Numerical Study, Materials 15 (13) (2022) 4394. Accessed 29 August 2022].

[67] Huang, H., Qian, C., Zhao, F., Qu, J., Guo, J. and Danzinger, M. (2016) Improvement on microstructure of concrete by polycarboxylate superplasticizer (PCE) and its influence on durability of concrete. [online]. 110, pp. 293–299. [Accessed 27 June 2023].

[68] R. Suryanita, H. Maizir, R. Zulapriansyah, Y. Subagiono, M.F. Arshad, The effect of silica fume admixture on the compressive strength of the cellular lightweight concrete, *Results Eng.* [Online] 14 (2022) 100445.

[69] Reni Suryanita, EXPERIMENTAL STUDY ON PERFORMANCE OF CELLULAR LIGHTWEIGHT CONCRETE DUE TO EXPOSURE HIGH TEMPERATURE, online 21 (83) (2021). Accessed 26 June 2023].

[70] R. Bajpai, K. Choudhary, A. Srivastava, K.S. Sangwan, M. Singh, Environmental impact assessment of fly ash and silica fume based geopolymer concrete, *J. Clean. Prod.* [Online] 254 (2020) 120147.

[71] K.H. Yim, F.S. Nahm, K.A. Han, S.Y. Park, Analysis of Statistical Methods and Errors in the Articles Published in the Korean Journal of Pain, Korean J. Pain. 23 (1) (2010) 35–41, https://doi.org/10.3344/kjp.2010.23.1.35.

[72] Núñez-Regueiro, M. (2015). Yaşlı Kadınlarda Üreme Sağlığı. DergiPark (*Istanbul University)*, 1(1). doi:⟨https://doi.org/10.1016/j⟩.

[73] M.A. Musarat, W.S. Alaloul, M.S. Liew, A. Maqsoom, A.H. Qureshi, Investigating the impact of inflation on building materials prices in construction industry, J. Build. Eng. 32 (2020) 101485, https://doi.org/10.1016/j.jobe.2020.101485.

[74] A. Krishna Rao, D.R. Kumar, Effect of various alkaline binder ratio on geopolymer concrete under ambient curing condition, Mater. Today.: Proc. (2020), https://doi.org/10.1016/j.matpr.2020.03.682.

[75] S.H. Ghasemzadeh Mousavinejad, M.F. Gashti, Effects of alkaline solution to binder ratio on fracture parameters of steel fiber reinforced heavyweight geopolymer concrete, Theor. Appl. Fract. Mech. 113 (2021) 102967. Accessed 5 April 2022].

[76] Mohd Ahmed, J. Mallick, Mohd Abul Hasan, A study of factors affecting the flexural tensile strength of concrete, *J. King Saud. Univ. - Eng. Sci.* [Online] 28 (2) (2016) 147–156.

[77] R. Vinai, A. Rafeet, M. Soutsos, W. Sha, The Role of Water Content and Paste Proportion on Physico-mechanical Properties of Alkali Activated Fly Ash–Ggbs Concrete, J. Sustain. Metall. 2 (1) (2015) 51–61, https://doi.org/10.1007/s40831-015-0032-6.

[78] EN1, Sustain. Constr. Works— Assess. Environ. Perform. Build. —Calc. Method 5978 (2011).

[79] G. Saini, U. Vattipalli, Assessing properties of alkali activated GGBS based self-compacting geopolymer concrete using nano-silica, *Case Stud. Constr. Mater.* [Online] 12 (2020) e00352. Accessed 24 July 2020].

[80] Hammond, G., Jones, C., Lowrie, Ed. fiona and Tse, P. (2011) A BSRIA guide: Embodied Carbon, The Inventory of Carbon and Energy(ICE).

[81] D.J.M. Flower, J.G. Sanjayan, Green house gas emissions due to concrete manufacture, Int. J. Life Cycle Assess. 12 (5) (2007) 282–288.

[82] B. Udvardi, A. Hamza, Emese Kurovics, István Kocserha, R.óbert Géber, A. Simon, Production of lightweight geopolymer concrete, 012045–012045 1527 (1) (2020), https://doi.org/10.1088/1742-6596/1527/1/012045, 012045–012045.

[83] T.Y. Lo, H.Z. Cui, Effect of porous lightweight aggregate on strength of concrete, Mater. Lett. 58 (6) (2004) 916–919, https://doi.org/10.1016/j.matlet.2003.07.036.

[84] M.-H. Zhang, O.E. Gjørv, Microstructure of the interfacial zone between lightweight aggregate and cement paste, Cem. Concr. Res. 20 (4) (1990) 610–618, https://doi.org/10.1016/0008-8846(90)90103-5.

[85] D. Simoes, Felipe, A. Lúcia, Verônica Scarpini Candido, Rios, C., Fabio and Sergio Neves Monteiro, Comp. Anal. Prop. Microstruct. geopolymeric Concr. Portland Concr. 7 (4) (2018) 606–611. ⟨https://doi.org/10.1016/j.jmrt.2018.08.008⟩ (doi).

[86] C. Ng, U.J. Alengaram, L.S. Wong, K.H. Mo, M.Z. Jumaat, S. Ramesh, A review on microstructural study and compressive strength of geopolymer mortar, paste and concrete, Constr. Build. Mater. 186 (2018) 550–576, https://doi.org/10.1016/j.conbuildmat.2018.07.075.

[87] A. Wang, Y. Zheng, Z. Zhang, K. Liu, Y. Li, L. Shi, D. Sun, The Durability of Alkali-Activated Materials in Comparison with Ordinary Portland Cements and Concretes: A Review, Engineering 6 (6) (2020) 695–706, https://doi.org/10.1016/j.eng.2019.08.019.

[88] Markeset G.: "Failure of concrete under compressive strain gradients". Bulletin No.110 (PhD Thesis), Norwegian Institute of Technology, Department of Structural Engineering, University of Trondheim, Trondheim, Norway,1993, 168 pp.

[89] M. Shariq, J. Prasad, H. Abbas, Creep and drying shrinkage of concrete containing GGBFS, Cem. Concr. Compos. 68 (2016) 35–45, https://doi.org/10.1016/j.cemconcomp.2016.02.004.

[90] ASTM C512/C512M-10 (2010), *Standard test method for creep of concrete in compression,* ASTM international, West Conshohocken (PA).

[91] Y. Xu, J. Liu, J. Liu, P. Zhang, Q. Zhang, L. Jiang, Experimental studies and modeling of creep of UHPC, Constr. Build. Mater. 175 (2018) 643–652, https://doi.org/10.1016/j.conbuildmat.2018.04.157.

[92] V.Y. Garas, K.E. Kurtis, L.F. Kahn, Creep of UHPC in tension and compression: Effect of thermal treatment, Cem. Concr. Compos. 34 (4) (2012) 493–502, https://doi.org/10.1016/j.cemconcomp.2011.12.002.

[93] C. Pang, W. Zheng, Y. Wang, W. Chang, Analysis and Modelling of Shrinkage and Creep of Reactive Powder Concrete, 732–732, Appl. Sci. 8 (5) (2018), https://doi.org/10.3390/app8050732.

[94] S.-H. Hong, J. Choi, T. Yuan, Y.-S. Yoon, A review on concrete creep characteristics and its evaluation on high-strength lightweight concrete, J. Mater. Res. Technol. 22 (2023) 230–251, https://doi.org/10.1016/j.jmrt.2022.11.125.

[95] D. Shen, J. Jiang, J. Shen, P. Yao, G. Jiang, Influence of prewetted lightweight aggregates on the behavior and cracking potential of internally cured concrete at an early age 99 (2015) 260–271, https://doi.org/10.1016/j.conbuildmat.2015.08.093.

[96] A. Wendling, K. Sadhasivam, R.W. Floyd, Creep and shrinkage of lightweight self-consolidating concrete for prestressed members, Constr. Build. Mater. 167 (2018) 205–215, https://doi.org/10.1016/j.conbuildmat.2018.02.017.

[97] Steenie Edward Wallah (2006). *Creep and Drying Shrinkage Behaviour of Low-Calcium Fly Ash-Based Geopolymer Concrete*.

[98] E. Negahban, A. Bagheri, J. Sanjayan, One-Year study of restrained shrinkage and creep behaviours of geopolymer concrete, Constr. Build. Mater. 376 (2023) 131057, https://doi.org/10.1016/j.conbuildmat.2023.131057.

[99] C. Seneviratne, Chamila Gunasekara, Sujeeva Setunge, D. Robert, Creep, shrinkage and permeation characteristics of geopolymer aggregate concrete: long-term performance, Arch. Civ. Mech. Eng. 20 (4) (2020), https://doi.org/10.1007/s43452-020-00119-w.

[100] K. Sagoe-Crentsil, T. Brown, A. Taylor, Drying shrinkage and creep performance of geopolymer concrete, J. Sustain. Cem. -Based Mater. 2 (1) (2013) 35–42, https://doi.org/10.1080/21650373.2013.764963.